Weather forecasting of meteorological variables for Moscow and Moscow Region

L.V. Berkovich, Yu.V. Tkacheva, V.A.Shnaydman *
Hydrometeorological Research Center of Russia
E-mail: lberkov@ mecom.ru
*Rutgers University, New Brunswick, New Jersey
E-mail: volf@ envsci.rutgers.edu

The Dynamical Weather Forecasting System (DWFS) operated at the Hydrometeorological Research Centre of Russia [1,2,3]. Its outputs are the short-range 48-h predictions of:

- surface meteorological variables (temperature, humidity, and wind velocity);
- cloud amount and precipitation rates; and
- vertical profiles of wind, temperature, and turbulence characteristics in the 2 km layer .

The skill of DWFS we demonstrate here by verification statistics of its improvement over the persistence (forecast error- FE and persistence error – PE) [4] . The corresponding data on temperature, precipitation, and wind predictions for Moscow in 2001 are given in Table which reproduces the mean absolute forecast error of daily minimum and daily maximum temperatures ($\delta T_{\min}$, $\delta T_{\max}$; °C), 12-h precipitation amount (δP_r , mm), and wind speed (δV, m·s^{-1}). We demonstrate the improvement of our weather forecasts over persistence, because there are no currently available another objective short-range weather forecasting techniques for Moscow, which we could compare our forecasts with. Operational forecasts calculated from operational database for 17 Russian cities around Moscow demonstrate about the same skill as shown in Table for Moscow.

	δT_{min}	δT_{max}	δP_r			δV			
	Projection (h)								
	0-36		00-12	12-24	24-36	12	24	36	48
FE	1.7	2.0	1.4	1.5	1.8	1.5	1.7	1.8	1.9
PE	2.7	2.8	2.7	2.3	2.6	2.0	1.8	2.4	2.2

.

A description is provided of basic concepts, prediction techniques, and performance of a system for operational short-range forecasting of meteorological variables and weather patterns at the Russian Hydrometeorological Research Centre. The basic principle of the system lies in reconstruction of both synoptic-scale and mesoscale weather patterns from the output product of a large-scale prediction model by means of the ABL model algorithms and locally-adapted parameterizations of the radiative heating effects on the near-surface air temperature variation as well as of some other physics. The system provides quite realistic 48 h guidance of weather patterns for cities in Russia and for a limited area encompassing Russia, Eastern Europe, and neighbouring regions. Detailed prediction for different parts of the city of Moscow and its suburbs is provided as well.

As it is shown, DWFS has considerable operational effectiveness. Further improvements and developments being partly in progress now are:

- improvement of the air humidity prediction through implementation of a simplified land surface hydrology model;
- implementation of a moist convection model for prediction of convective precipitation to replace the currently used semi-empirical technique;
- parameterized treatment of the impact of atmospheric fronts upon the evolution of meteorological variables in the boundaru layer and free atmosphere;
- development of optimal parameterizations for treatment of dynamical and thermal characteristics and radiative balance of the underlying surface to account for spetial features of the builtup areas in various parts of a large city; and
- development and implementation of parameterized treatment of the anthropogenic heating impacts to improve the technique of detailed weather forecasting for a large city.

REFERENCES

1. Berkovich L.V., Belousov S.L., Kalugina G.Yu, Tkacheva Yu.V. Developments in the short-term dynamical weather forecasting system at the Hydrometeorological Research Center of Russia. – Res.Act. in Atmos. And Oceanic Modeling, 1999, No.28, 5.7-5.8.
2. Berkovich L.V., Belousov S.L , Tkacheva Yu.V. Operational hydrodynamical forecasting of meteorological variables and weather patterns for locations in Russia and contiguous countries. – Russian Meteorology and Hydrology, 1998, No.4, 11-22.
3. Berkovich L.V , Tarnopolskiy A.G., Shnaidman V.A. A hydrodynamic model of the atmospheric and oceanic boundary layers. – Ibid., 1997, No.7, 30-40.
4. Belousov S.L., Berkovich L.V., V.A.Shnaydman. Short-range forecasting of meteorological variables and weather patterns. – Res.Act. in Atmos. And Oceanic Modeling, 2001, No.31, 5.1-5.2.

The Australian Tropical Cyclone Limited Area Prediction System

Noel E. Davidson[1] and Gordon E. Jackson[2]

[1] *Bureau of Meteorology Research Centre,*
PO Box 1289K, Melbourne, Victoria, 3001, Australia
[2] *RSMC Darwin, Bureau of Meteorology,*
13 Scaturchio St, Casuarina 0810, Northern Territory, Australia
N.Davidson@bom.gov.au ; G.Jackson@bom.gov.au

The Tropical Cyclone Limited Area Assimilation and Prediction System (TC-LAPS) became operational for the 1999-2000 Australian tropical cyclone season. Details of the system are described in Davidson and Weber (2000).

TC-LAPS has five basic components: (a) Data assimilation to establish the storm's large-scale environment (LSE) and outer structure. (b) Vortex specification to construct the inner core circulation and asymmetries consistent with the estimated size, intensity and past motion. (c) High-resolution (HR) analysis, with appropriate observational errors, length scales and quality control tolerances, to merge the intense vortex into the LSE. (d) Initialisation with diabatic, dynamical nudging, to balance the vortex and insert satellite-defined cloud asymmetries. (e) High-resolution prediction with the generalised LAPS forecast model (Puri *et al*., 1998), which contains high order numerics and sophisticated physical parameterisations.

Data Assimilation and Coarse Resolution Configuration
The LSE assimilation is based on a standard 6-hour analysis-forecast cycle with a multivariate statistical interpolation analysis. It uses standard observational data obtained in real time from the GTS and local satellite temperature retrievals and cloud drift winds. Synthetic moisture profiles obtained from GMS infrared imagery enhance the moisture analysis. Real time sea surface temperature analyses based on weekly collections of ship and satellite data are used.

Domain - Large Scale Environment (LSE):	55.0°S–56.75°N, 70.0°E-164.75°W
Assimilation cycle:	6 hour cycle
Horizontal resolution:	0.75° (150x170 lat-lon grid)
Vertical resolution:	19 sigma levels from 0.991 to 0.05
Analysis Method:	Multi-variate Statistical Interpolation
Analysed Variables:	Geopotential and wind fields
Initialisation:	Digital Filter
Nesting:	Lateral boundary at 6-hour intervals from operational global model
Soil Moisture Analysis:	Daily 0.25°x 0.25° over Australia. Fortnightly 0.8°x 0.8° climatology elsewhere
Sea Surface Temperature Analysis:	Weekly 1.0°x1.0°
GMS Bogus Moisture data:	6 hourly 0.5°x0.5°
GMS Cloud Top Temperature data:	Hourly 0.5°x0.5°

Vortex Specification and Initialisation
Construction of the TC vortex is based on a TC advisory issued by RSMC Darwin on the past motion and structure of the storm. A symmetric vortex is constructed using an empirical surface pressure profile, assuming a moist adiabat at the TC centre, and empirical relations to define the mass field between the centre and the LSE. The wind field is obtained by gradient wind balance. A wave number one asymmetry is constructed such that the observed drift speed equals the sum of the environmental flow and the flow induced by the artificial asymmetry at the observed vortex centre. The synthetic vortex is implanted into the global analysis after filtering to remove any previously existing, weak and misplaced circulation. Synthetic observations are produced at high horizontal resolution to define the inner core structure. 24 hours of diabatic, dynamical nudging is used to balance the vortex and re-define the vertical motion field to be consistent with the satellite cloud imagery.

High Resolution Forecast Model
The TC-LAPS system is double-nested, with the LSE nested within the global forecast, and the HR relocatable domain, centred on the TC, nested within the LSE forecast.

Domain – High Resolution (HR):	Variable 27°x27°, TC centred
Horizontal resolution:	0.15° (180x180 lat-lon grid)
Analysis Method:	Univariate Statistical Interpolation
Vertical resolution:	19 sigma levels from 0.991 to 0.05
Initialisation:	24 hours diabatic, dynamical nudging
Nesting:	Boundary conditions at 3-hour intervals derived from +0 to +72 hour LSE forecasts.

Physical Parameterisations and Surface Grid Fields

Convection:	Earlier version of ECMWF's Mass-flux
Large scale rain:	Supersaturation Scheme
Boundary Layer:	Earlier version of ECMWF's VB Scheme
Short Wave Radiation:	3-hourly, Lacis and Hansen
Long Wave Radiation:	3-hourly, Fels and Schwarzkopf
Topography:	Derived from 0.1^o resolution data
Soil Moisture Analysis:	Daily 0.25^ox 0.25^o over Australia. Fortnightly 0.8^ox 0.8^o climatology elsewhere
Sea Surface Temperature Analysis:	Weekly 1.0^ox1.0^o
Albedo:	Climatology

Verification

The following statistics are for the 2001 North West Pacific season. In situations where multiple storms were present, the principal storm at the base time of the forecast was verified (until November 2001, only one forecast to 48 hours was made per base time).

Total number of TCs verified = 16
Chebi, Durian, Utor, Trami, Kong-Re, Toraji, Man-Yi, Pabuk, Danas, Nari, Vipa, Francis,Lekima, Krosa, Haiyan, Podul

(i) Track errors

Forecast Interval	No. Cases	Error (km)
T+00	117	20.8
T+24	110	138.7
T+48	89	236.9

(ii) Central pressure errors (hPa)

Forecast Interval	No. Cases	**RMS Error**		Mean Error		Abs Error	
		TC-LAPS	**Persistence**	TC-LAPS	Persistence	TC-LAPS	Persistence
T+00	117	**6.5**	**0.0**	-5.0	0.0	5.4	0.0
T+24	110	**11.0**	**13.7**	-5.6	-3.6	8.7	11.0
T+48	89	**16.6**	**21.8**	-10.0	-8.2	13.2	18.0

Operational Output

TC-LAPS now runs over a high-resolution TC centred domain, twice a day to T+72h, based on data valid at 00 and 12 UTC. It can be run twice, centred on two separate systems for both time periods.

Track forecasts are produced within the high-resolution domain out to 72 hours using an automated vortex tracking routine that locates the centre from the MSLP and low-level wind fields. This produces centre location, central pressure and the maximum wind below 850 hPa.

Other guidance products for 6-hourly periods out to 72-hours from TC-LAPS are made available through registered user access to the Darwin RSMC web page at:

http://www.bom.gov.au/weather/nt/rsmc/

These products include:

- MSLP;
- Winds at 950, 850, 700, 500, 250, 200 hPa;
- 24-hour precipitation;
- Forecast and observed track.

References

Davidson, N.E. and H. C. Weber, 2000: The BMRC High-Resolution Tropical Cyclone Prediction System: TC-LAPS. *Mon. Wea. Rev.*, ***128***, 1245–1265.

Puri, K., G.S. Dietachmayer, G.A. Mills, N.E. Davidson, R.A. Bowen and L.W. Logan, 1998: The new BMRC Limited Area Prediction System, LAPS. *Aust. Meteor. Mag*., **47**, 203-223.

Short-Term Downscaling with a Limited-Area Model: Diagnostic Verification in a Perfect-Model Approach

Ramón de Elía, René Laprise *, and Bertrand Denis
Département des sciences de la Terre et de l'Atmosphère, Université du Québec à Montréal

1. Introduction

Nested limited-area models (LAMs) have been used by the scientific community for a long time with the implicit assumption that they are able to generate meaningful small-scale features that were absent in the initial and in the lateral boundary conditions. A number of studies in the past have evaluated the validity of the mentioned hypothesis, with a variety of results (e.g. Anthes et al., 1985). In spite of the lack of conclusive results in this area, it is commonly argued that LAMs simulate meaningful mesoscale features (Peagle et al., 1997).

The experiment carried out in de Elia et al.(2002) increased the evidence that challenges this widespread notion. For doing this, a perfect-model approach was followed. A high-resolution large-domain LAM was driven by global analyses producing a long simulation that was used to drive a high-resolution small-domain LAM. Spatial filtering to remove the fine scales in the driving data provided to the small-domain LAM (as lateral boundary and initial conditions) was performed in order to mimic the low-resolution atmospheric fields that usually drive LAMs. This setup permitted a comparison between the simulations of both LAMs over the same region. Results showed that the small-domain LAM was incapable of reproducing the small scales present in the large-domain LAM with the precision required by a root-mean-square (RMS) measure of error for most of the length scales removed by filtering.

As discussed in de Elia et al.(2002), comparisons between forecast (small domain) and reference run (large domain) through the use of RMS might be too demanding to fairly evaluate results. It is well known that the RMS is highly sensitive to phase errors. It has been argued several times that even when models score very badly in terms of RMS, forecasters have benefited from the information provided by these models. For this reason, in this study an attempt to use a less stringent measure is intended. In addition, the scale analysis that was a natural sophistication of the RMS study, is abandoned in order to put more emphasis into the physical space. The reason is that localized small-scale systems loose representativeness in a spectral approach, and hence, large values in a spectral RMS error may hide successful predictions of important phenomena.

The technique used in this analysis is derived from the "Diagnostic verification" developed by Murphy and Winkler (1987), and it consists in a distribution-oriented approach. Although familiarity with it would facilitate the understanding of this note, it is not essential.

2. Experimental framework

The Canadian Regional Climate Model (CRCM) described in Caya and Laprise (1999) is used for a series of simulations with 45-km horizontal grid spacing, 18 levels in the vertical, and a 3-h nesting frequency. A first integration is made for a month in a domain of 196x196 grid points in the horizontal (centered in New England), nested with NCEP analyses of February 1993. This high-resolution simulation reference run becomes our "truth" to which other runs will be compared to.

The output fields produced by this reference run are then filtered to remove smaller scales in order to simulate a low-resolution dataset. These low-resolution fields are then used to drive simulations performed over a smaller domain (100x100 in the horizontal, keeping the vertical and horizontal resolution untouched) located in the centre of the larger domain. This setup permits the comparison of the output of both simulations in the same region and therefore assesses the ability of the one-way nesting to reproduce the results of the larger domain. Since both simulations use the same formulation (dynamics, physics, resolution, numerics, etc), differences in results can be attributed unambiguously to the nesting technique.

In order to make values statistically stable, results were obtained for 24 runs of the small-domain model integrated during 4 days, each one starting on successive days of February 1993. In this way, for example, the 48-hour integration ensemble average, implies the average over 24 different 48-hour integrations, one day apart. A more detailed description of this experiment can be found in de Elia et al. (2002).

3. Results

For reasons of brevity, only results from 96-hour integration for vorticity at 850 hPa are presented. An enhanced scattergram is displayed in Fig. 1. Pairs of points from both the forecast and the reference runs at each grid point and for all 24 runs are considered to build the distributions represented in the diagram. Following the ideas discussed by Murphy and Winkler (1987), it is possible to think this diagram in terms of conditional and marginal distributions. Histograms of the forecast and reference variables are represented at

* *Corresponding author address:* René Laprise, Sc. Terre-Atmosphère, UQAM Salle PK-6528 B.P. 8888, Succ. Centre-ville Montreal, QC, Canada H3C 3P8. e-mail: laprise.rene@uqam.ca

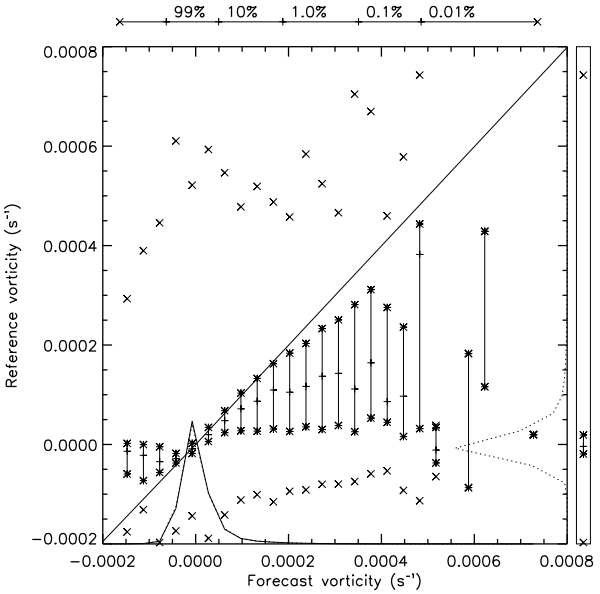

Figure 1: *Conditional and marginal distributions for large- and small-domain 850-hPa vorticity fields after 96-hour integration.*

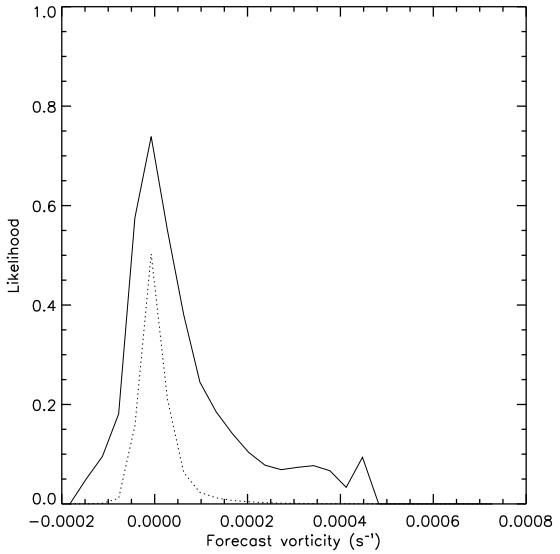

Figure 2: *Likelihood of success for small-domain integration (solid line) and random forecasts (dotted line).*

the sides without scale. In the same way, values in the scattergram are thought of as belonging to distributions of the reference values conditional to the forecast values. These distributions are represented following a standard way denoting the extremes (with an "X"), the first and third quartile (with asterisks connected by a line), and finally the median (with a dash). Used together, these symbols divide each distribution in quarters.

It can be seen in the histograms that the maximum amount of data in both the forecast and the reference run occurs around zero vorticity. It can also be seen that both distributions are virtually identical. This is somewhat expected since both fields were generated with the same model, although in different grids. It is worth noting that the similarity of distributions between large- and small-domain runs suggests an unbiased statistics (identical averages, variances, etc.).

The figure also shows that, for larger values of forecast vorticity, the conditional distributions tend to be biased towards lower values of the reference vorticity, while interquartile distances become longer (larger variance). This should not be interpreted as an inability of the model of producing high levels of vorticity (as we have discussed in the previous paragraph, the model is unbiased), but simply as the inability of producing it at the right place. The conditional bias towards lower values appear because high vorticity levels are a low probability phenomena, and when wrongly forecasted, tend to be replaced with more common phenomena (lower levels of vorticity, as seen in the histogram).

It is very illuminating to compare the likelihood of obtaining the right solution with this forecast model and with a random generator with the same statistics. This can be done by using the distributions already obtained and ignoring the estimation problem. Figure 2 displays the likelihood of obtaining the right forecast, within a given interval, for the small-domain run (solid line) and for the random forecast (dashed line). As we can see the small-domain run performs always better than the random model, although its likelihood becomes small for large vorticity values and hence of dubious utility.

4. Conclusions

It is clear from these results that, although the 96-hour forecast is by no means deterministic, the small-domain runs generate solutions whose distribution provides more information than the one obtained with the random model. This probability of success is notably increased if the verification allows a phase error of 1 or 2 grid points (not shown). These results are more optimistic than those of de Elia et al. (2002) discussed in the introduction, although both are derived from the same set of data. Less stringent constraints as well as a more meteorological approach may explain the difference. These results tend to confirm also the advantage of the probability framework even for interpreting Limited-Area Models.

References:

Anthes et al., 1985; *Advances in Geophysics*, Vol. 28, 159-202.

Caya, D. and R. Laprise, 1999; *Mon. Wea. Rev.*,**127**, 341-362.

de Elia, R., R. Laprise, and B. Denis, 2002: submitted to *Mon. Wea. Rev.*.

Murphy, A.H., and R.L. Winkler, 1987; *Mon. Wea. Rev.* ,**115**, 1330-1338.

Paegle at al., 1997; *Meteor. Atmos. Phys.*, **63**, 53-69.

NUMERICAL SIMULATION OF HEAVY SNOWFALL SYSTEMS OBSERVED ON THE SOUTHERN COASTAL AREA OF SEA OF JAPAN ON 16 JANUARY 2001

Hisaki Eito*, Teruyuki Kato and Masanori Yoshizaki

Meteorological Research Institute, Japan Meteorological Agency, Tsukuba, Japan

1. INTRODUCTION

On 12-16 January 2001, a heavy snowfall was observed in Joetsu area, the western part of Niigata prefecture, Japan(in Fig. 1). The snow depth on the ground increased 1 m 40 cm deep during 5 days in Joetsu city. The snowfall was mainly induced by quasi-stationary band-shaped snowfall systems. They elongated east and west along the southern coast of sea of Japan. In this study, we tried to reproduce this snowfall system using a cloud resolving model, and investigated its structure and environmental field.

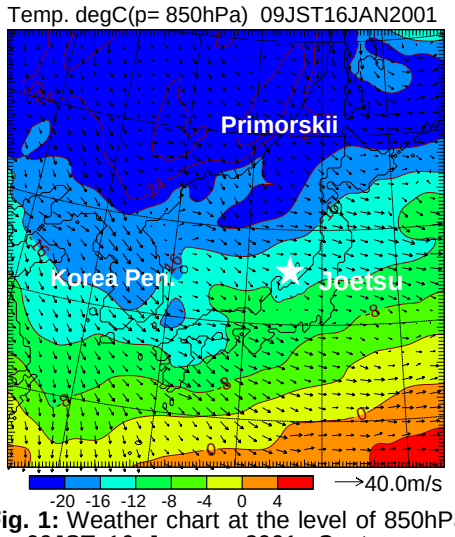

Fig. 1: Weather chart at the level of 850hPa on 09JST 16 January 2001. Contours and arrows denote temperature (deg C) and wind vector field respectively. Star mark presents the location of Joetsu city.

2. OBSERVATIONS

Fig. 1 shows the air temperature and wind fields at the level of 850hPa on 09JST 16 JAN. 2001. A continental strong cold air had flowed out over Sea of Japan. Two major cold air streams were seen. One is mainly north-westerly flow from Primorskii to the northern part of Japan, another is mainly westerly flow from Korea Pen. to the western part of Japan. Joetsu area is located down the former stream.

A remarkable snowband was observed in Joetsu area on 16 January by JMA Niigata operational radar. Fig. 2a shows a horizontal distribution of hourly precipitation intensity deduced from radar at 1400JST. This snowband was about 200km in length and about 50km in width and aligned in an east and west direction at coastal area. Fig. 2b shows a temporal variation of precipitation intensity along 138E in Fig.2a. This snowband was quasi-stationary during a whole day and caused 40cm snowfall in Joetsu city.

Corresponding author address: Hisaki Eito,
Meteorological Research Institute,
Japan Meteorological Agency,
Nagamine, Tsukuba, Ibaraki 305-0052, Japan,
E-mail: heito@mri-jma.go.jp

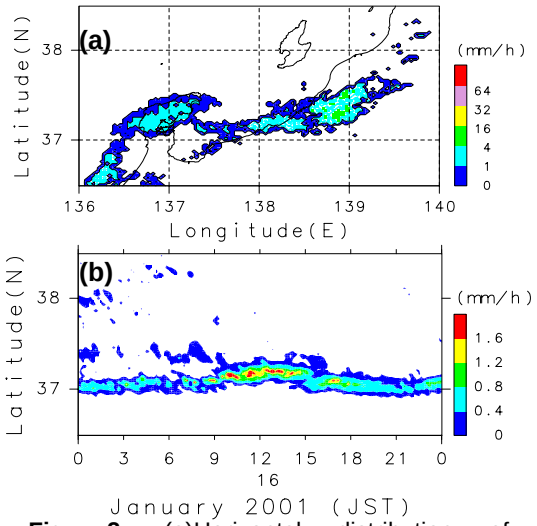

Fig. 2: (a)Horizontal distribution of precipitation intensity observed by the JMA Niigata operational radar at 1400JST 16 January 2001. (b)Time-latitude (along 138E in (a)) cross section of precipitation intensity.

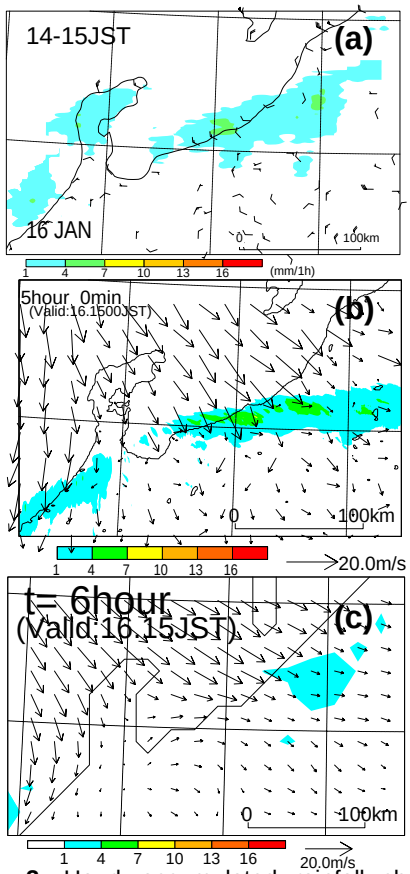

Fig. 3: Hourly-accumulated rainfall charts from 1400JST to 1500JST on 16 January 2001. (a) Observation, (b) 1km-NHM simulation, and (C) RSM simulation.

3. NUMERICAL MODELS

The elastic version of the Meteorological Research Institute/Numerical Prediction Division,JMA unified nonhydrostatic model (MRI/NPD-NHM: Saito et al. ,2001) was used. The calculation domain has 300x300x38 horizontal and vertical grids. The cloud-physics in the model contains the cold rain scheme. The MRI-NHM with a 1-km horizontal grid(1km-NHM) is one-way nested within the forecast of the MRI-NHM with a 5-km grid(5km-NHM). The initial and boundary conditions for a 5km-NHM are provided from output produced by Regional Spectral Model(RSM), which is a hydrostatic model used operationally in the Japan Meteorological Agency. The 5km-NHM is one-way nested within the RSM forecast with the initial time 09JST 16 Jan.2001.

4. RESULTS

4.1 STRUCTURE OF SNOWBAND

Fig. 3 shows hourly-accumulated snowfall charts form 1400JST to 1500JST. The snowfall areas and intensity simulated by the 1km-NHM (Fig.3b) well corresponded with the observations(Fig. 3a), while the RSM with a 20-km grid simulated the intensity considerably weaker and the area broader(Fig. 3c).

Fig. 4 shows the horizontal distribution of snow mixing ratio simulated by the 1km-NHM between 1400JST on 16 January 2001 (4 hour forecast). The convective cells in the simulated snowfall system, which are about 10km in horizontal scale and about 4km in vertical scale, propagate east-southeastward at a speed of about 10ms^{-1}. The direction and speed of cell's motion roughly correspond with those of the wind in the system. They spread in a eastward direction.

4.2 ENVIONMENTAL FIELD OF SNOWBAND

Fig. 5 shows the horizontal distribution of vertical difference of equivalent potential temperature between about a 1.2km height and the surface. On the northern side of the snowfall system, a convectively unstable atmosphere is observed in the lower layers, accompanying with the environmental winds that veered to the northwest toward the surface.

Fig. 6 presents the horizontal distribution of potential temperature and wind field near the surface. In the coastal area of Toyama and Ishikawa prefectures, a cold air pool is observed. The convergence zone is formed by a cold air outflow and the warmer northwesterly wind. The snowband developed over this convergence zone.

This simulation shows that the snowfall system formed as a result of convectively unstable marine atmosphere in the lower layers from the northwest flowing into the coastal convergence region. The convective cells in the system were carried to the downwind side by the mean wind in the system, and developed by the inflow of convectively unstable atmosphere in the lower layer from the northern side of this system.

5. SUMMARY

By using the cloud resolving model nested in the operational regional model, observed features of the band-shaped heavy snowfall system was well reproduced. The system contained several convective cells with about a 10km length and about a 4km height. The inflow of convectively unstable marine atmosphere in the lower layers were significant for the formation and maintenance of these snowfall system

Reference

Saito, K., T. Kato, H. Eito and C. Muroi, 2001: Documentation of the Meteorological Research Institute/ Numerical Prediction Division Unified Nonhydrostatic Model. *Tec. Rep. MRI*, **42**, 133 pp.

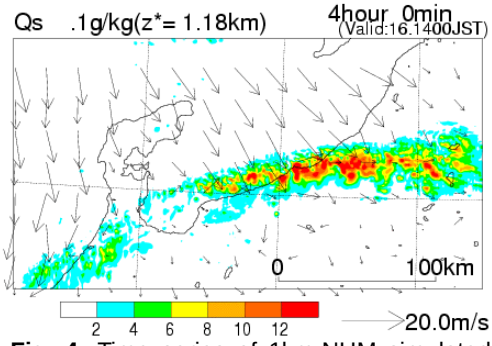

Fig. 4: Time series of 1km-NHM simulated snow mixing ratio (0.1g/kg) at z*=1.18km with surface horizontal wind vectors between 1400JST(4hour forecast) and 1450 JST (4hour 50min forecast) with 10 minutes.

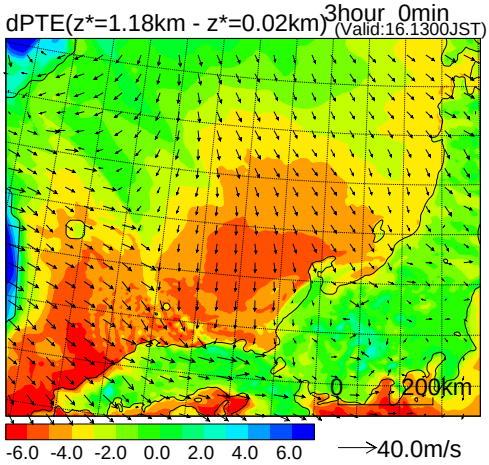

Fig. 5: 5km-NHM simulated horizontal distribution of vertical difference of equivalent potential temperature between about 1.2km height and surface on 1300JST 16 January 2001(3 hour forecast). White and black vector denote horizontal wind at about 1.2km height and surface, respectively.

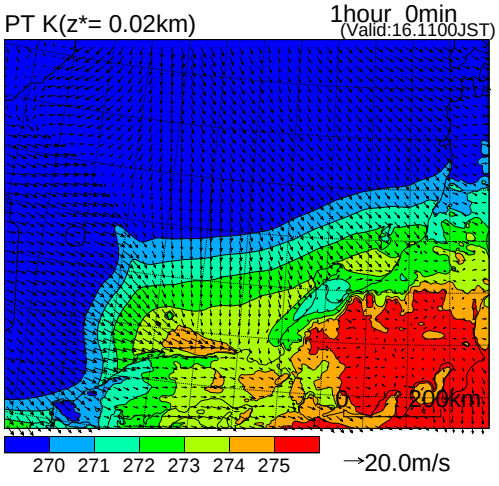

Fig. 6: 5km-NHM simulated horizontal distribution potential temperature at surface on 1100JST 16 January 2001 1 hour forecast). Vector denotes horizontal wind at surface.

MM5 10-M WIND DIRECTION FORECAST SKILL OVER BAY OF BENGAL DURING SPRING 2001

Pat J. Fitzpatrick, Gueorgui V. Mostovoi and Yongzuo Li
Engineering Research Center, MSU, Stennis Space Center, Mississippi
E-mail: mostovoi@erc.msstate.edu

Skill of 10-m wind direction forecasts produced by the PSU/NCAR mesoscale model (MM5, Dudhia, 2001) is evaluated during March and April 2001. For the verification 10-m wind speed and direction retrieved from the microwave scatterometer QuikSCAT (QSCAT, 2001) measurements are used. QSCAT data represent values averaged over 25x25 km cells. The MM5 is integrated with a resolution of 27 km and 30 vertical levels are used. The model integration domain is limited by 0.38N-33.8N and by 32.7E-105.6E. Boundary conditions are provided by NCEP AVN forecasts and "cold start" option is used. QSCAT data is available over Bay of Bengal around 00Z and 12Z time. Thus the quality only of 12, 24 and 36 hours MM5 forecasts started at 00Z and 12Z are evaluated. Selection procedure of QSCAT winds involves time filtering and choosing the "best quality" data followed by bilinear interpolation to 1-degree latitude-longitude grid. For the comparison with NOGAPS (Hogan, Rosmond, 1991) forecasts MM5 output also interpolated to 1x1° grid.

An example of a wind direction bias error (model – observed) distribution averaged for March-April period and for 12-hour forecast time is shown in Fig. 1a for MM5 and in Fig. 2b for NOGAPS. There is a clear tendency for a positive wind direction bias for both models along East Coast of India, approximately from 12°N to 20°N. In contrast, over the NE part of Bay of Bengal a negative wind direction bias is observed. Simulated air's flow over this part of Bay of Bengal tends to be directed more towards land than the observed flow. In general, a positive wind direction bias is observed over Andaman Sea and Gulf of Martaban. For quantifying the relative improvement of MM5 10-m wind direction on mean absolute direction error (*ADE*) as follows:

$$SS_{ADE} = \left(1 - \frac{ADE_{MM5}}{ADE_{NOGAPS}}\right)100 .$$

The mean *ADE* for NOGAPS is used as an accuracy measure of a reference forecast.

Geographical distribution of the skill score is depicted in Fig. 2a for 12 h forecast and in Fig. 2b for 24 h. MM5 forecasts show a region of a clear improvement (positive SS values) in 10-m wind direction prediction over Gulf of Martaban. It's important to note that 10-m wind direction error depends on an observed speed. Generally a low wind speed is associated with a large (> 60° and more) direction error. At a relatively high speed (> 5 m/s) a direction error has a tendency to became as small as 30-40° or less. This relationship between a wind direction error and observed speed for both models is well illustrated by Fig. 3b and Fig. 3c.

References

Dudhia J. et. al., 2001: PSU/NCAR Mesoscale Modeling System Tutorial Class Notes and User's Guide: MM5 Modeling System Version 3. - Mesoscale & Microscale Meteorology Divison NCAR.

Hogan T., and T. Rosmond, 1991: The description of the Navy Operational Global Atmospheric Prediction System's spectral forecast model. *Mon. Wea. Rev.*, **119**, 1786-1815.

QSCAT, 2001: Remote Sensing Systems' Database for Satellite Microwave Data. [Available online at ftp://ftp.ssmi.com/QSCAT].

Wilks D.S., 1995: Statistical Methods in the Atmospheric Sciences. Academic Press, 467 pp.

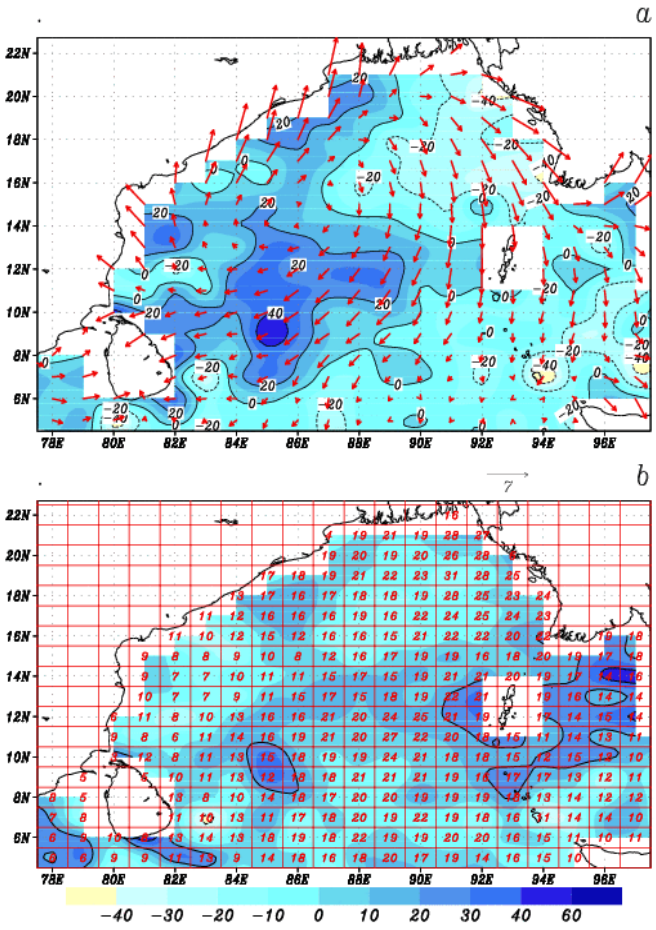

Fig. 1. Mean wind direction bias for March-April 2001 MM5 (a) and NOGAPS (b) forecasts started at 00Z. Averaged QSCAT . wind field is shown by arrows. Digits correspond to the number of cases used for averaging

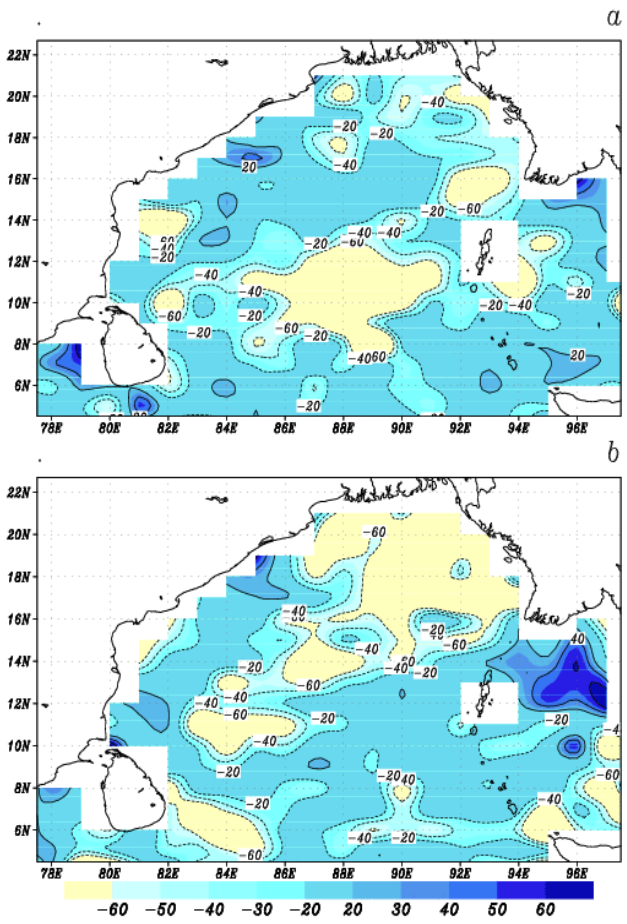

Fig. 2. Geographical distribution of MM5 10-m wind direction skill score against NOGAPS for 12 h (a) and for 24 h (b) forecasts

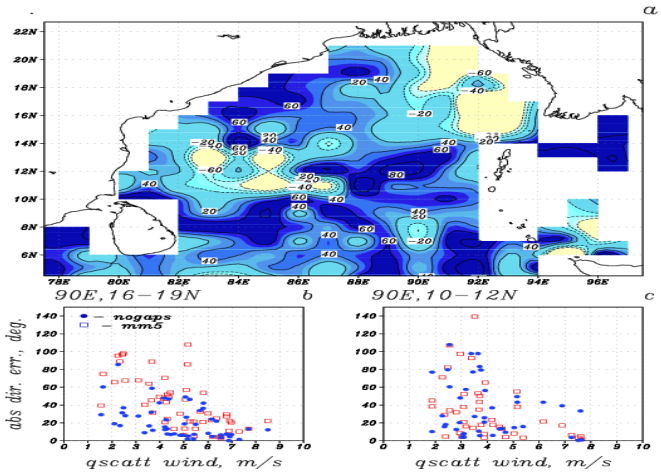

Fig. 3. Same as Fig. 2b, but only for cases with observed wind speed > 5 m/s. Relationship between observed wind speed and absolute direction error for two sample regions: (90-91E,16-19N) (b) and (90-91E,10-12N) (c).

MM5 10-M WIND DIRECTION FORECAST SKILL OVER BAY OF BENGAL DURING SUMMER MONSOON PERIOD 2001

Pat J. Fitzpatrick, Gueorgui V. Mostovoi and Yongzuo Li
Engineering Research Center, MSU, Stennis Space Center, Mississippi
E-mail: mostovoi@erc.msstate.edu

Skill of 10-m wind direction forecasts produced by the PSU/NCAR mesoscale model (MM5, Dudhia, 2001) is estimated from June to August 2001. The same estimation methodology and the same MM5 configuration as described in a paper of Fitzpatrick et al. (2002) are used. The evaluation is made over Bay of Bengal. Over this region 10-m wind speed and direction retrieved from the microwave scatterometer QuikSCAT (QSCAT, 2001) measurements are available around 00Z and 12Z.

The distribution of 10-m wind direction bias error (model – observed) averaged for June-August 2001 is shown in Fig. 1a for 12 h and in Fig. 1b for 24 h forecast. In two regions behind Sri-Lanka MM5 and global NOGAPS (Hogan, Rosmond, 1991) model demonstrate a substantial positive wind bias (> 40). Both models predict surface flow directed more offshore than observed.

A relative improvement of MM5 10-m wind direction forecasts over NOGAPS in terms of the skill score based on absolute direction error (Fitzpatrick et al., 2002) is shown in Fig. 2a for 12h and Fig. 2b for 24 h forecast. One can see that MM5 produces positive skill mainly along NE India coastline (from 16N to 20N), close to the eastern edge of Sri Lanka and along the equatorial belt up to 5-6N. It is found that an absolute direction error depends on the wind speed value over coastal waters. The small direction errors are associated with relatively strong winds as shown in Fig. 3b. In contrast there is no any relationship between wind direction error and observed speed over an open Ocean (see Fig. 3c).

References

Dudhia J. et. al., 2001: PSU/NCAR Mesoscale Modeling System Tutorial Class Notes and User's Guide: MM5 Modeling System Version 3. - Mesoscale & Microscale Meteorology Divison NCAR.

Hogan T., and T. Rosmond, 1991: The description of the Navy Operational Global Atmospheric Prediction System's spectral forecast model. *Mon. Wea. Rev.*, **119**, 1786-1815.

Fitzpatrick P., Mostovoi G. & Li Y., 2002: MM5 10-m wind direction forecast skill over Bay of Bengal during spring 2001. *Research Activities in Atmospheric and Oceanic Modeling*, see current Report.

QSCAT, 2001: Remote Sensing Systems' Database for Satellite Microwave Data. [Available online at ftp://ftp.ssmi.com/QSCAT].

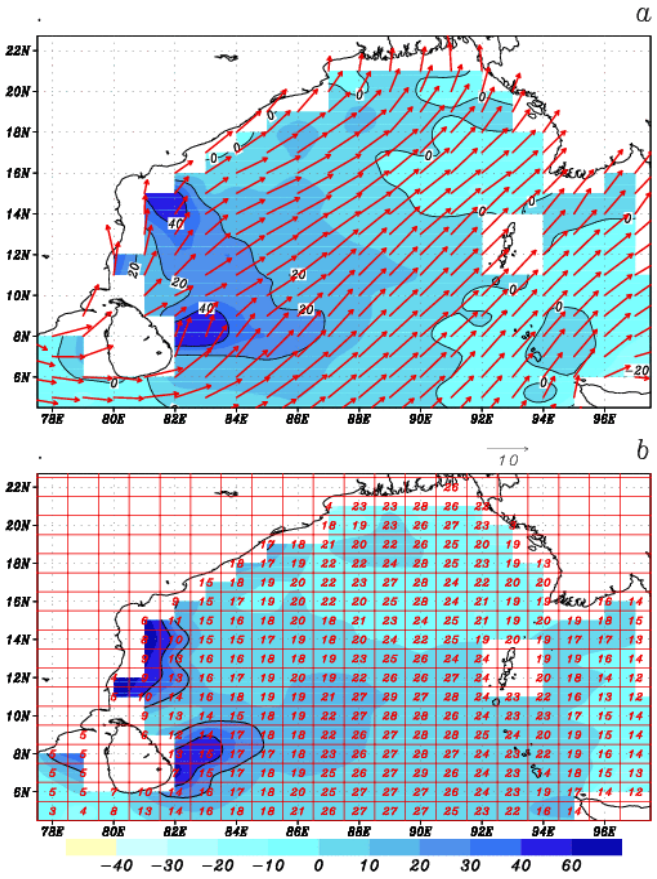

Fig. 1. Mean win direction bias for June-Augustl 2001 MM5 (a) and skill NOGAPS (b) forecasts started at 00Z. Averaged QSCAT wind field is shown by arrows. Digits correspond to the number of cases used for averaging

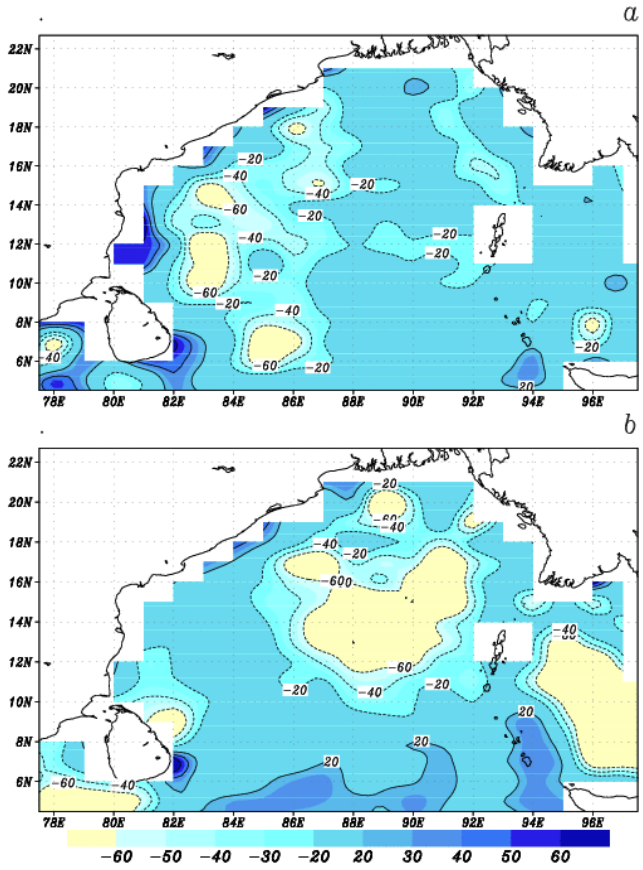

Fig. 2. Geographical distribution of MM5 10-m wind direction score against NOGAPS for 12 h (a) and for 24 h (b) forecasts.

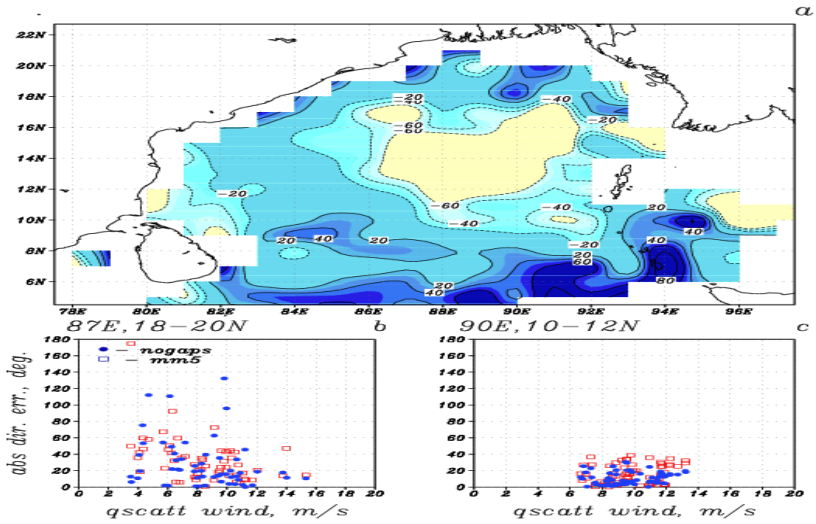

Fig. 3. Same as Fig. 2b, but only for cases with observed wind speed >9 m/s. Relationship between observed wind speed and absolute direction error for two sample regions: (86-87E,18-20N) (b) and (90-91E,10-12N) (c).

Evaluation of summer-time near-surface temperature and wind fields over Hudson Bay in a regional atmospheric model

Philippe Gachon[1], François J. Saucier[1] and René Laprise[2]
[1]*Maurice Lamontagne Institute, Ocean Sciences Branch,*
Department of Fisheries and Oceans,
850 route de la Mer, Mont-Joli, Qc, Canada G5H 3Z4
[2] *Department of Earth & Atmospheric Sciences, University of Québec at Montréal, Montréal, Qc, Canada*
e-mail : gachonp@dfo-mpo.gc.ca

The Hudson Bay (HB) climate system is dominated by the presence of a seasonal sea ice cover over 8 months per year. This has a considerable effect on the regional climate (i.e. on the mesoscale atmospheric circulation, e.g., Gachon, 1999, on precipitation variability and regime, continental permafrost, snow cover and the annual hydrological cycle) and biota (e.g. Gough and Wolfe, 2001). The relatively short ice-free period between the end of July early November is important in controlling the mixed-layer heat storage and the formation of sea ice in the fall.

In summertime, the sea surface temperature (SST) over the most part of HB is considerably cooler (typically from 1°C in the north to 10°C in the south) than the surrounding land surface temperature. The low-level air temperature is cooled by heat intake over the Bay. This produces a shallow low-level inversion that increases the near surface atmospheric stability over sea water. This has effects on humidity, temperature and wind profiles (see Figs 2a and 2b, respectively), as well as low-level clouds and radiation. Those in turn control the seasonal oceanic heating of the mixed layer.

The coupling of the Canadian Regional Climate atmospheric Model (CRCM described in Caya and Laprise, 1999) to a Hudson Bay ocean model (as described in Senneville et al., this volume) requires that each one reproduce vertical fluxes correctly. Herein we evaluate low-level temperature and wind fields as simulated by the CRCM for August 1996 (with a 25-km horizontal resolution and 40 layers in the vertical). The CRCM is driven by reanalyses from the Canadian forecast model (100-km resolution global grid archived every 6 hours) using daily observed SST and sea ice cover concentration (still present in western HB at the beginning of August, see Fig. 1). The land surface temperature is initialised on August 1st 1996 from the reanalyses. We examine the differences in screen-level temperature and anemometer wind speed between the high resolution reanalyses from the regional version of Canadian forecast model at a 35-km resolution (Mailhot et al., 1997) and the CRCM results over HB. The screen-level temperature is also compared with the meteorological observations at four stations over land near the eastern and northern HB shores (i.e. La Grande Rivière, Kuujjuarapik, Inukjuak, and Kuujjuaq, see Fig. 1). The screen-level temperature calculated by the CRCM is diagnosed from the surface temperature and that at the lowest model level as described in McFarlane et al. (1992). The wind at the 10 m anemometer level in the CRCM is diagnosed from the lowest prognostic level for momentum and using a bulk Richardson number criteria for stability function, such as the screen-level temperature (e.g. Boer et al., 1984; McFarlane et al., 1992).

As shown in Fig. 2a, the temperature above HB differs from the reanalysis and the CRCM results with large differences during the first six days of the month and at several times thereafter. During these periods, the CRCM is cooler than the reanalyses by 3 to 7°C with a strong dependence to the cold SST, which in turn reduces the variability of the CRCM low-level air temperature (see the SST and CRCM time series in Fig. 2a). Recall that both the reanalyses and the CRCM use the same SST (updated every day). As shown also in the wind speed (Fig. 2b), the CRCM simulates periods of calm (no winds) conditions compared to the reanalyses, but the strong wind events are reproduced similarly. The calm periods are associated with colder temperature in the CRCM (Fig. 2a). This is a result of enhanced near surface stability in the CRCM. These periods of calm conditions or underestimated wind speed in atmospheric models have also been found over other cold oceanic surface such as the Gulf of St. Lawrence in summer. This result points to the importance of future work on the boundary layer treatments in the CRCM, and the criteria used for calculating the wind at anemometer level. As suggested by Taylor (2001), the performance of bulk formulation as used in CRCM for simulating the near-surface turbulence fluxes, needs to be better established for stable conditions. This would require new data on vertical profiles over the HB.

Along the eastern shore, the CRCM results can be validated from the meteorological stations. The temperature evolution is relatively well reproduced (Fig. 3), but with a higher RMS error than the reanalyses (Table 1). As over HB, the temperature temporal variability is generally underestimated in the CRCM except for Inukjuak station (as shown in Table 1). At this station, the CRCM is more systematically warmer than at other stations (Fig. 3). This bias can in part be attributed to the use of a one layer only land surface sheme, as suggested in the previous work of Verseghy (1996) and the recent study over northern Québec of Frigon et al. (this volume). As for over sea, the analysis of a more complete set of terrestrial stations around the Bay with the CRCM results should improve the evaluation of the model, in particular in the western part of the Bay upstream of the HB influence.

Our study is at present too limited in scope to be definitive. However, it suggests that much work is required in the CRCM for estimating the screen-level fields and the surface exchanges processes over cold surfaces such as HB in summertime. This is true not only for future on-line coupling but also for off-line forcing of the ocean model as the mixed layer properties of HB are sensitive to the accuracy of atmospheric fields in summer months, as suggested in the preliminary studies of Senneville et al. (this volume).

References

Boer, G.J., N.A. McFarlane, R. Laprise, J.D. Henderson, and J.P. Blanchet. 1984 : The Canadian climate centre spectral atmospheric general circulation model. *Atmos. Ocean*, **22**, 397-429.

Caya, D., and R. Laprise. 1999. A semi-implicit semi-lagrangian regional climate model : The Canadian RCM. *Mon. Wea. Rev*., **127** : 341-362.

Gachon, P. 1999 : Effets de la distribution de la glace marine sur le développement des dépressions à méso-échelle et sur le climat régional, PhD's Thesis, University of Québec at Montréal (UQAM), Montréal (Québec, Canada), 352 p.

Gough, W.A., and E. Wolfe. 2001. Climate change scenarios for Hudson Bay, Canada, from General Circulation Models. *Arctic*, **54**, 2, 142-148.

Mailhot, J., R. Sarrazin, B. Bilodeau, N. Brunet, and G.

Pellerin. 1997. Development of the 35-km version of the Canadian regional forecast system. *Atmos.-Ocean*, **35**, 1-28.

McFarlane, N.A., G.J. Boer, J.P. Blanchet, and M. Lazare. 1992 : The Canadian climate centre second-generation general circulation model and its equilibrium climate. *J. Climate*, **5**, 1013-1044.

Taylor, P.K., Ed.. 2001. Intercomparison and validation of ocean-atmosphere energy flux fields. Joint WCRP/SCOR Working Group on Air-Sea Fluxes Final Rep., WCRP-112, WMO/TD-No, **1036**, 306 pp.

Verseghy, D.L.. 1996 : Local climates simulated by two generations of Canadian GCM land surface schemes. *Atmos.-Ocean*, **34(3)**, 435-456.

Fig. 1. Land-sea-ice mask used in the CRCM valid on August 1st 1996 (black is the land, light grey the open ocean, and white the sea ice).

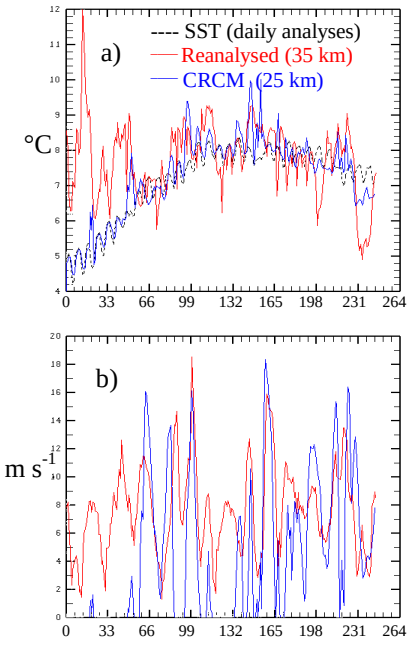

Fig. 2. Temporal evolution (every 3 hours) of (a) SST (daily analyses in dashed line) and air temperature (at 2 m, in °C) and (b) wind speed (at 10 m, in m s^{-1}) over HB for reanalysed (35-km grid) and CRCM values. X-axis corresponds to the 8 times daily archived fields (1-31 August 1996).

Temperature (°C)	Observed (ST)	Reanalysed (35 km)	CRCM (25 km)	
La Grande Rivière	6.46	5.89	5.21	ST
53.63°N-77.7°W		**1.95**	**3.71**	**RMS**
Kuujjuarapik	5.92	4.84	3.42	ST
55.28°N-77.77°W		**2.65**	**4.15**	**RMS**
Inukjuak	2.79	3.09	3.79	ST
58.47°N-78.08°W		**1.47**	**3.74**	**RMS**
Kuujjuaq	5.29	5.48	4.48	ST
58.1°N-68.42°W		**1.99**	**4.13**	**RMS**

Table 1. Standard deviation (ST) and Root Mean Square error (RMS, between observed and reanalysed, and observed and modeled) during August 1996 for temperature at terrestrial stations (see Fig. 1).

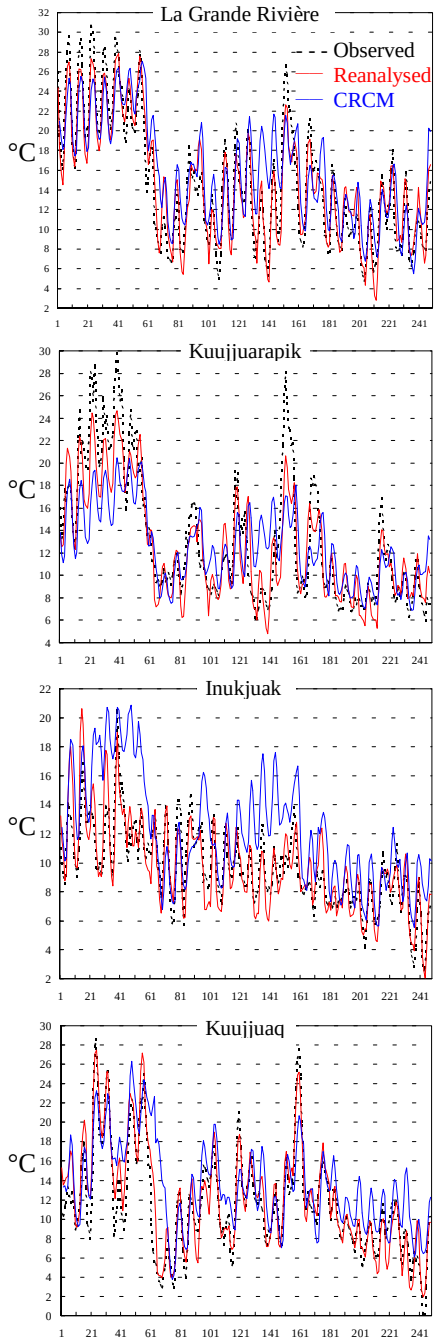

Fig. 3. As Fig. 2a but for the temporal evolution of temperature at terrestrial stations (shown in Fig. 1).

NWP research in Austria

T. Haiden
Central Institute for Meteorology and Geodynamics
thomas.haiden@zamg.ac.at

1. Operational forecast system

Operational limited area weather forecasts in Austria are made using version AL12 of the ARPEGE/ALADIN modelling system. Horizontal resolution is 10 km, the number of levels in the vertical is 31 (increased to 37 in 03/2002), domain size is ~1300x1100 km, covering central Europe. The model is spectral, run in hydrostatic mode, with a semi-implicit, semi-Lagrangian advection scheme. Initial and boundary conditions are taken from the ALADIN-LACE run at CHMI in Prague, which in turn is coupled to the global ARPEGE model. A modified Bougeault-type scheme is used for deep convection, a first-oder closure for turbulent vertical transports, and the ISBA (Interaction Soil-Biosphere-Atmosphere) scheme is used to represent surface processes. Coupling frequency is 6 hours in both cases. Integrations up to +48 hours are performed twice a day. Hourly analyses of surface fields are produced based on regional synop observations using optimum interpolation. Point verification statistics and verification of areal precipitation are computed quasi-operationally.

2. Research

a. Diurnally forced convection over land

A common problem in many NWP models is the timing of convective precipitation related to the diurnal cycle over land. Models typically show a too early onset of locally forced deep convection and associated rainfall. This behaviour was confirmed by case studies of mountain convection in the Alps under conditions of negligible synoptic forcing, using radar data for verification (Haiden, 2001). Whereas considerable forecast skill was found with regard to mesoscale variability of precipitation, onset time was consistently underestimated. Part of the problem is attributed to the mostly diagnostic character of current deep convection schemes. Therefore a prognostic scheme, allowing for some ‘memory’ of the intensity of convective updrafts, is being tested (Gerard, 2001). Preliminary results indicate that the delayed onset of convection in the new scheme is on the order of 1 hour, which is not sufficient to completely remove the timing bias.

b. Orographic precipitation downscaling

The prediction of flash flooding requires very fine scale precipitation forecasts both in space (~1 km) and in time (10 min). Because of nonlinear catchment response, peak runoff may be significantly understimated if LAM-scale rainfall rates are assumed to be homogeneously distributed across the catchment. The effect of both dynamical downscaling and statistical downscaling is tested on selected MAP events using the hydrological model WaSiM-ETH. Besides providing insight into the precipitation-runoff process in alpine catchments this method also offers a means of verification for LAM precipitation forecasts. Ahrens et al. (2001) found that the ALADIN-VIENNA operational resolution (9.6 km) gives rather good results in these cases. Increasing the resolution to 4 km does not show systematic improvement.

c. Scale-dependence of nonhydrostatic effects

The ARPEGE/ALADIN system allows for a straightforward switch between hydrostatic and nonhydrostatic versions. Based on theoretical analyses and idealized experiments it is generally acknowledged that non-hydrostatic effects must be taken into account on a resolution of 10 km and below. However, little is known about the effects of non-hydrostatic dynamics on actual model skill over realistic topography, in a quasi-operational model setting. A study is under way to perform a systematic evaluation of such effects for model resolutions down to 2.5 km (Stadlbacher, 2001).

d. Statistical and dynamical adaptation

In Nov 2002, the 2nd SRNWP Workshop on Statistical and Dynamical Adaptation will be held in Vienna. Presentations are invited about research in NWP statistical adaptation (MOS, PPM, Kalman filtering), dynamical adaptation, and neural network methods. The program also includes research on the use of ensemble predictions in statistical/dynamical post-processing.

References

Ahrens, B., H. Seidl und K. Jasper, 2001: On the validation of ALADIN quantitative precipitation forecasts in an Alpine catchment. *MAP Newsletter,* **15**, 57-60.

Gerard, L., 2001: Physical parameterizations for a high resolution operational numerical weather prediction model. University of Brussels, Ph.D. Thesis.

Haiden, T., 2001: Orographically triggered convection: a case study. Proceedings, *10th ALADIN Workshop*, Toulouse, France.

Stadlbacher, K., 2001: Systematic qualitative evaluation of a high-resolution non-hydrostatic model. *ALADIN Newsletter*, **19**, 42-43.

THE AUSTRALIAN AIR QUALITY FORECASTING SYSTEM

G. D. Hess[1], M. E. Cope[2,3], S. Lee[2], P. C. Manins[2], P. Nelson[3], K. Puri[1], K. Tory[1], N. Wong[4], and M. Young[5]

[1]Bureau of Meteorology Research Centre, Melbourne, Victoria, Australia, [2]CSIRO Atmospheric Research, Aspendale, Victoria, Australia, [3]CSIRO Energy Technology, North Ryde, New South Wales, Australia, [4]Environment Protection Authority of Victoria, Melbourne, Victoria, Australia, [5]New South Wales Environment Protection Authority, Lidcombe NSW, Australia. E-mail: d.hess@bom.gov.au

The recent advances in supercomputing have opened up a number of new areas of potential applications for meteorological forecasting. One such area is numerical air quality forecasting. It is now possible to combine a high-resolution meteorological model with a high-resolution air quality model to forecast the concentrations of various pollutant species at a spatial resolution comparable to the size of suburbs. However, increasing the detail of the air quality forecast from the scale of the urban airshed down to the scale of suburbs brings with it a whole new set of scientific problems and challenges.

The Australian Air Quality Forecasting System (AAQFS) is a joint project between the Bureau of Meteorology (BoM), CSIRO Atmospheric Research (CAR), CSIRO Energy Technology (CET), the Environment Protection Authority of Victoria (EPA-VIC) and the New South Wales Environment Protection Authority (NSW EPA) to develop a high-resolution air quality forecasting system. The initial development of AAQFS was funded by the Air Pollution in Major Cities Program (sponsored by Environment Australia). Currently 24-36 hour forecasts are produced in both Melbourne and Sydney. The System was trialled in a Demonstration Period from August 2000 – July 2001 (which included the 2000 Olympics and Para-Olympics in Sydney and the 2000-2001 summer oxidant season).

The project has a number of specific goals: to provide the ability to generate 24-36 hour air quality forecasts twice per day (available 9 am and 3:30 pm); provide forecasts for a range of air pollutants including oxides of nitrogen (NO_x), ozone (O_3), sulfur dioxide (SO_2), carbon monoxide (CO), benzene (C_6H_6), formaldehyde (CH_2O) and particulate matter (PM10 and PM2.5); provide forecasts at a resolution sufficient to consider suburban variations in air quality; and to provide the ability to generate simultaneous forecasts for a 'business-as-usual' emissions scenario and a 'green emissions' forecast. The latter scenario may correspond to minimal motor vehicle-usage and will be used to indicate the reduction in population exposure that could result from a concerted public response to a forecast of poor air quality for the next day.

The AAQFS consists of five major components: a numerical weather prediction (NWP) system, an emissions inventory module (EIM), a chemical transport module (CTM) for air quality modelling, an evaluation module, and a data archiving and display module (data package).

The BoM's operational Limited Area Prediction System (LAPS) system has been adapted for the AAQFS NWP component. Comprehensive numerics and physics packages are included and recent work has paid special attention to the resolution and treatment of surface processes. The model has 29 vertical levels and a horizontal resolution of 0.05° (covering the state of Victoria and most of New South Wales). This model is nested in LAPS at 0.375° resolution, which in turn is nested in the BoM global model, GASP.

EPA-VIC and CSIRO, with support from NSW EPA, have developed the emissions inventory. The inventory uses size-fractionated and speciated particle emissions, 0.01° gridded area sources over the densely populated regions and meteorologically dependant emissions that are generated based on LAPS predictions. Recent innovations include updating the emissions model for wood-burning heaters; implementing and testing a wind-blown dust model; developing and testing a power-based vehicle emissions model developed to generate road-specific vehicle emission fluxes for the purpose of near-road impact modelling; and the introduction of the beginnings of a bushfire modelling component.

The CTM has been custom built for the project using state-of-the-art methodologies. A notable inclusion to the CTM is the Generic Reaction Set (GRS) photochemical mechanism, a highly

condensed (7 species and 7 reactions) photochemical transformation mechanism featuring minimal computational overhead. Testing is going on to update this model to include 12 species and 14 reactions. Particle transformation is modelled by a sectionally based particle scheme. The transport fields are updated every 60 minutes. The CTM has 17 vertical levels and simulations use a 0.05° outer grid, with nested 0.01° inner grids for major urban areas.

Both the meteorological and air quality forecasts are the subject of on-going and case-specific validation. This is done through comparison of LAPS meteorological fields with METAR/SYNOP (near-surface) and AMDAR (vertical profiles from commercial aircraft) data and meteorological observations from the EPA monitoring networks. Air quality forecasts are compared to 1-hour EPA observations for NO_x (both as NO and NO_2) and O_3. This has been expanded to include SO_2, PM10, PM2.5, CO and, where available, non-methanic hydrocarbons. Critical to the validation process has been the availability of EPA data sets by the end of each forecast period, enabling the on-going validation to be substantially automated.

Data archiving is in NetCDF data packets, which are accessible via GUI-driven Q&A software. Sufficient information is available in a data packet to enable the CTM to be run offline at a later time. The EPAs have access to the daily forecasts via the AAQFS Web Site and manage the dissemination of the forecast data.

A public-access website, making all of the AAQFS reports available, is currently under construction; for further details, contact: d.hess@bom.gov.au.

The interaction of synoptic-scale and mesoscale flows is particularly important in forecasting air quality in Melbourne and Sydney. Figures 1 and 2 show two examples. Figure 1 shows a sea breeze, which formed in the late morning/early afternoon due to the land-sea temperature contrast, and was opposed by the westerly-northwesterly synoptic flow. The model was able to simulate this observed interaction (Fig. 1). Figure 2 shows predicted NO_2 concentrations advected by the Melbourne Eddy that forms in the lee of the mountains to the northeast of Melbourne when stable stratification forces the air to flow around the topography, rather than over it. Observations confirmed the model simulation of this clockwise circulation.

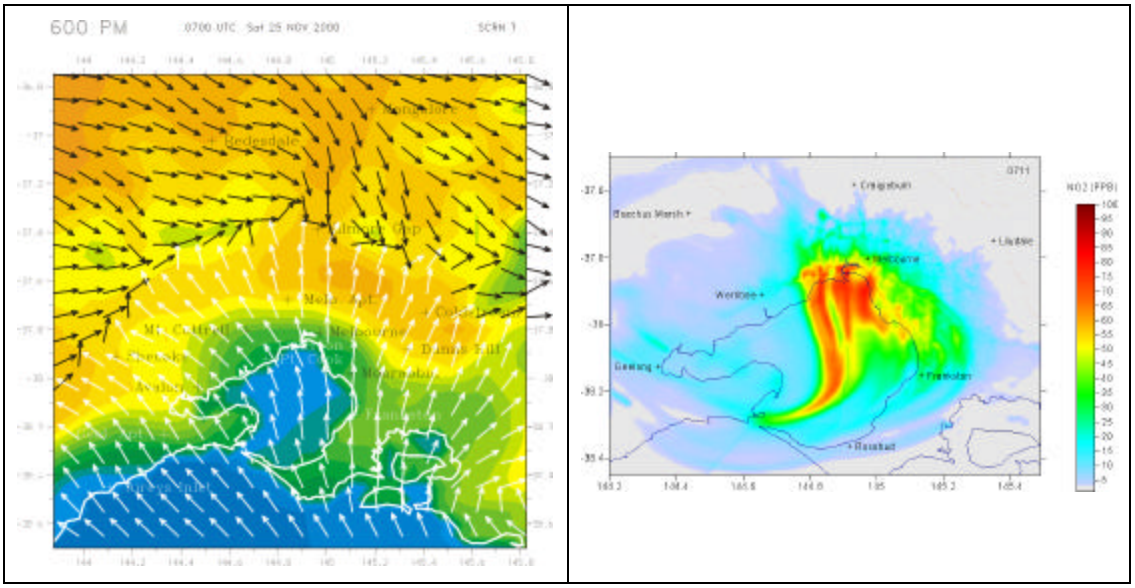

Fig. 1. Forecast of the sea breeze (white vectors) at 1800 EDT on 25 November 2000 in Melbourne showing the opposing synoptic flow. The background colour indicates screen temperature; blue is cool, yellow-green is warm, orange is hot.

Fig. 2. Forecast NO_2 concentrations at 1100 EDT 07 March 2001. Note that the NO_2 plume has been rotated clockwise by the Melbourne Eddy centred to the east of Geelong.

Hazardous Weather Phenomena Forecast In GIS Meteo Technology.

Iouri Ioussoupov
MapMakers Group Ltd., Moscow, Russia, E-mail: usupov@mapmak.mecom.ru.

The GIS Meteo technology was developed in MapMakers Group Ltd. for use in meteorologist's operational work [1]. In this paper a new tool for hazardous weather phenomena forecast based on a model of explosive cyclogenesis is represented.

The concept of isentropic potential vorticity (IPV) [3] is increasingly being applied in theoretical and synoptic studies of explosive cyclogenesis [2]. When positive (in Northern hemisphere) PV anomalies move over low-mid tropospheric front (baroclinic band), and in case of low stability in troposphere, explosive cyclogenesis may be occurred. Extensive positive upper level PV anomaly should produce a cyclonic rotation at the earth's surface, in this case in a low-level baroclinic band. The low-level circulation begins to produce and enhance regions of warm and cold advection in the lower levels. A low-level PV anomaly is now present due to the warming and the low-level vorticity. This circulation associated with this low-level PV anomaly is felt through the entire troposphere and into the stratosphere. The upper portion of this effect helps to amplify the upper level PV anomaly. This strengthening upper PV anomaly, in turn, strengthens the surface anomaly and so on (mutual amplification). This results in a fast fall of pressure on a surface, with accompanying storm winds, heavy precipitation etc. Our software can fully automatically calculate the locations, where explosive cyclogenesis may be predicted. The finding possible explosive cyclogenesis zones algorithm is shown below:

1. Calculate IPV anomalies.
   $$PV = g\,(f + \zeta_\theta) \bullet (-\partial\theta / \partial P)$$
2. Determine the frontal zones in troposphere using the Huber-Pock and Kress method [4].
3. Define the stability in troposphere by calculation of the Total Totals index.

When all these conditions are met the software determines a hazardous weather zone at this location. We have investigated 40 cases of hazardous weather phenomena since June 1998 to Febriary 2002, and in 38 cases the result was successful. There were cases of Moscow storm (21 June 1998 and July 2001), Paris storm (26-27 of December 1999), S. Petersburg (July, 15, 2000, July 16, 2001), Strasbourg (July 7, 2001) and many others. It should be noted, that meteorological offices didn't predict some of these cases at the time. As input data we used GRIB data distributed by WMO. Below you can see some meteorological maps prepared by GIS Meteo technology.

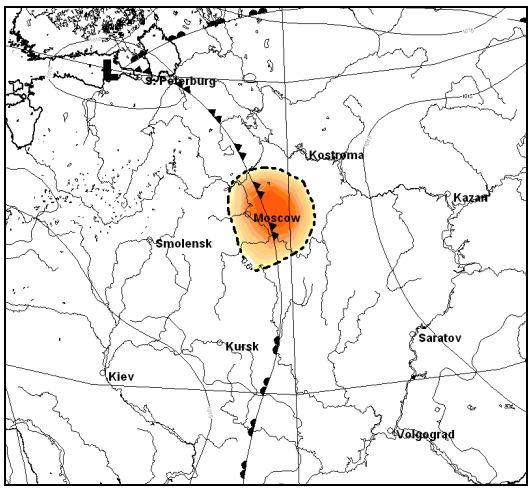

1998 / 06 / 21 00 UTC

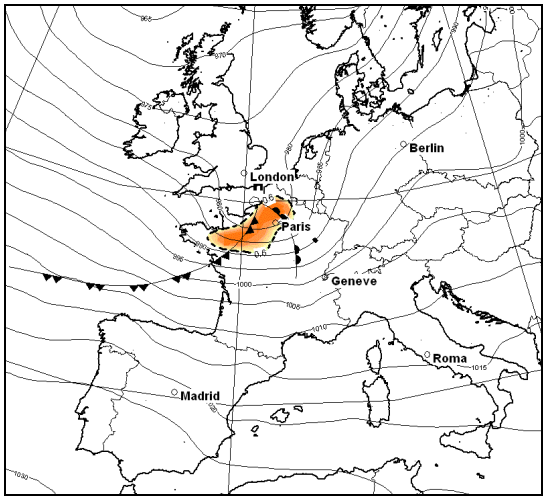

1999 / 12 / 26 06 UTC

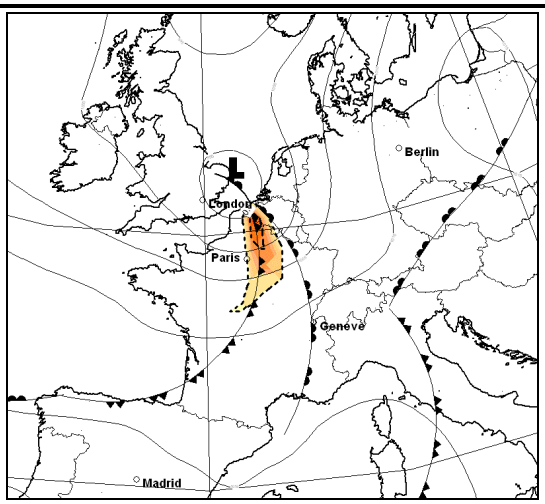

2000 / 05 / 28 12 UTC

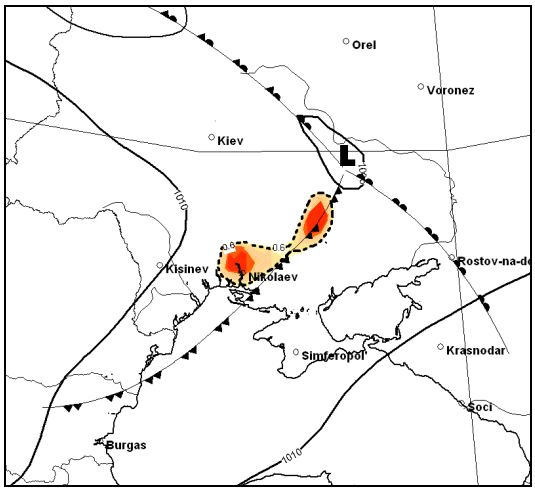

2000 / 07 / 06 06 UTC

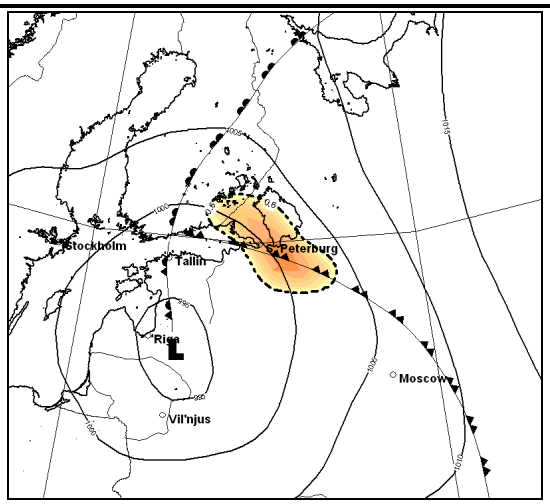

2000 / 07 / 15 18 UTC

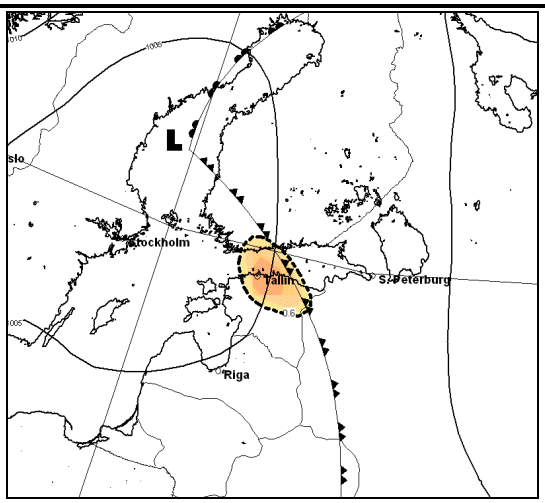

2001 / 07 / 19 06 UTC

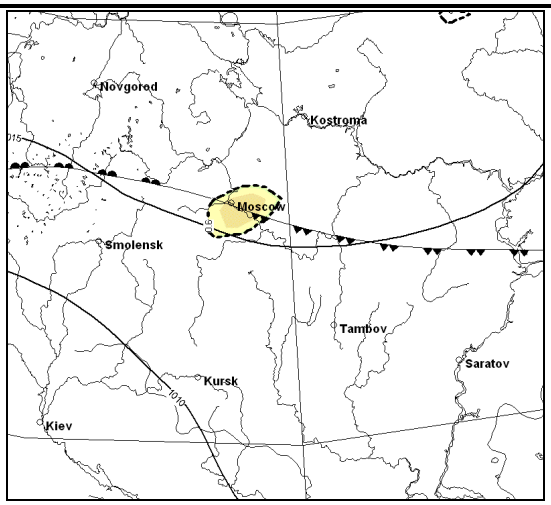

2001 / 07 / 24 12 UTC

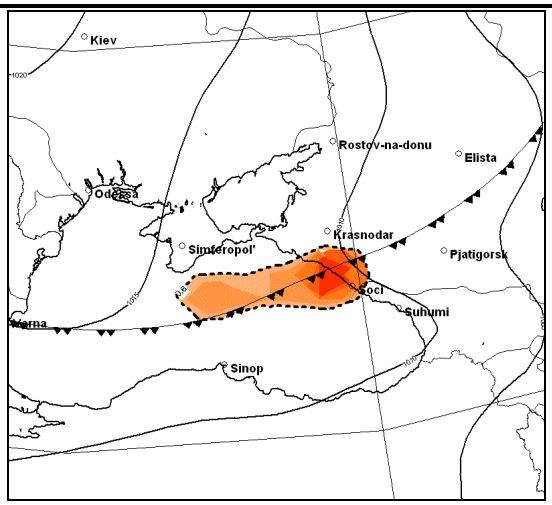

2001 / 09 / 26 12 UTC

References.

1. Akulinicheva A. A., Berkovich L. V., Solomakhov A. I., Shmelkin Y. L., Ioussoupov I. I. The Geographical Information System of Meteo and its usage in meteorological offices in Russia and formed CIS countries. – Meteorology and Hydrology, 2001, №11, P. 90-98.
2. Georgiev C. G. Quantitative relationship between Meteosat WV data and positive potential vorticity anomalies: a case study over the Mediterranean. Meterol. Appl., -1999, N 6, P. 97-109.
3. Hoskins B. J., McIntyre M. E & Robertson A. W. On the use and significance of isentropic potential vorticity maps. Q.J.R. Meteorol. Soc., -1985, N 111. P. 877-946.
4. Huber-Pock F., Kress Ch. An operational model of objective frontal analysis based on ECMWF products. Meteorol.Atmos. Phys. – 1989. – Vol.40, N 2. –P.170-180.

Photochemical Smog Investigations with a Parallel Version of the Mesoscale Model GESIMA

Hartmut Kapitza
Dieter P. Eppel
Institute for Coastal Research
GKSS Research Centre
21502 Geesthacht
Germany

The atmospheric mesoscale model GESIMA (**GE**esthacht **SI**mulation **M**odel of the **A**tmosphere) has been developed in the early 90's and successfully applied to a wide range of problems, e.g. sea-breeze studies, pollutant transport, wind energy evaluation studies. For a brief summary of features, references, availability, and a list of external users visit the GESIMA web site at http://w3g.gkss.de/staff/kapitza/gesima.

In a pilot study (Bauer 2000) a chemical reaction and transport module has been implemented to simulate photochemical smog episodes. The combined chemistry-atmosphere model was validated with data from an extensive field campaign showing very promising results. The chemistry module is now being integrated into the official community version of GESIMA to be made available to all interested users.

Furthermore, there is ongoing activity to implement GESIMA on distributed memory computer architectures (SMP machines or workstation clusters) using a public domain message passing library (MPI).

Verification of QPF for 5km-NHM predicted precipitation amount and area in Kanto Area, Japan

Teruyuki Kato*

Meteorological Research Institute, 1-1 Nagamine, Tsukuba, Ibaraki, 305-0052, Japan

1. Introduction

The Quantitative Precipitation Forecast (QPF) of Meteorological Research Institute / Numerical Prediction Division unified nonhydrostatic model (MRI/NPD-NHM; Saito et al, 2000) has been verified by Kato et al (1998). However, they examined the QPF of 10 km-model only during the monsoon season in Kyushu, southwestern part of Japan. In near future, MRI/NPD-NHM plans to be used as the operational mesoscale model of Japan Meteorological Agency (JMA). Thus, the purpose of this study is to verify the QPF of MRI/NPD-NHM with a higher resolution for a longer period. This verification can clarify some problems in MRI/NPD-NHM. The verification is made for the rainfalls observed in Kanto Area, middle part of Japan between January and December in 2000.

2. Numerical models and verification method

The 5km-resolution of MRI/NPD-NHM (5km-NHM) made an 18-hour forecast twice a day. The initial conditions of 5km-NHM were produced by interpolating the 3-hour forecasts of the operational regional model of JMA (RSM). The boundaries were also made by the forecast of RSM. Microphysics including the ice-phase was used as a precipitation scheme. No convective parameterization scheme was incorporated. The domain and terrain of models are shown in Fig. 1. The verification was made for the predicted total precipitation amount and area in comparison with Radar-AMeDAS analyzed rainfall (R-A). As shown by red rectangle in Fig. 1b, the verification area is divided into mountainous (i.e., above a height of 125 m), plain, and sea regions to examine the effect of terrain.

3. Monthly averaged total precipitation amount and area

Monthly averaged total precipitation and area of R-A, RSM, and 5km-NHM in the whole verification area are shown in Fig.2. The precipitation area is classified by precipitation intensity. Total precipitation amount predicted by RSM is larger than twice of that estimated by R-A. This is caused from the overestimation of weak rainfall less than 10mm h^{-1}. 5km-NHM also overestimated the precipitation by 1.8 times larger than R-A.

Noted that in the summer season the precipitation of 5km-NHM almost agrees with that of R-A. The characteristic features found in the summer are remarkable in the mountainous region. This agreement is resulted from the 5km-NHM having predicted some thunderstorms that occurred in the mountainous region.

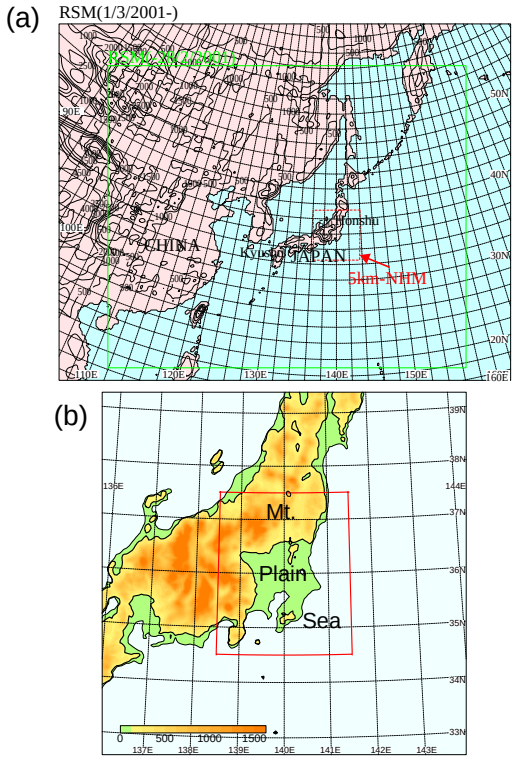

Fig.1 Domain and terrain of (a) RSM and (b) 5km-NHM. Red rectangle of (b) is the verification area.

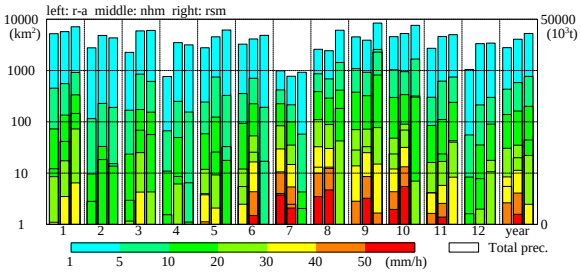

Fig.2 Monthly averaged total precipitation and area classified by precipitation intensity.

*Corresponding author address: Teruyuki Kato, Meteorological Research Institute, 1-1 Nagamine, Tsukuba, Ibaraki 305-0052 Japan: e-mail: tkato@mri-jma.go.jp

4. Reproductibity of diurnal variation

Diurnal variation of averaged total precipitation amount estimated by R-A has the maximum at 08-09 UTC (in the evening) on land, and at 19-20 UTC (in the early morning) on the sea. 5km-NHM successfully reproduced this characteristic features, while the reproductibity of RSM is not good (especially in the mountainous region). This is resulted from the high resolution of 5km-NHM that can express the fine terrain.

In the diurnal variation of precipitation area with intensity larger than 30mm h^{-1}, the maximum appears at 08-11UTC in the mountainous region, and at 12-13UTC in the plain region. This is caused by the movement of precipitation systems from the mountainous to plain regions. 5km-NHM well reproduced the maximum in the mountainous region, but the predicted rainfall in the plain region is considerably small.

Since no hydrometeor was given in the initial conditions of 5km-NHM, some stand up time of precipitation is taken. This time is estimated to be about 3 hours.

5. Verification results

Figure 3 shows the correlation coefficients of total precipitation amount and area predicted by 5km-NHM and RSM in the whole verification region against those of R-A. The prediction accuracy of total precipitation Pamount and area with intensity less 10mm h^{-1} is better for RSM than 5km-NHM. This is found in the all divided regions. The good correlation coefficients of RSM are resulted from the overestimation of the weak precipitation. It is remarkable that the accuracy of 5km-NHM becomes wrong with time, while the decrease of accuracy is small for RSM. This decrease is largest in the plain region (Fig.4).

6. Conclusion

MRI/NPD-NHM has good accuracy for the prediction of precipitation with intensity larger than 20mm h^{-1}. Especially, the accuracy for the rainfall in the mountainous region is considerably better than that of RSM. However, as pointed out by Kato et al (1998), the accuracy for the prediction of weak precipitation is not good for 5km-NHM. In the future, the overestimation of predicted total precipitation amount must be examined. This may be caused by the use of forecasts of RSM as initial and boundary conditions. Further, the effect of precipitation scheme, i.e., whether the single use of microphysics for a 5km grid is O.K. or not, must be studied.

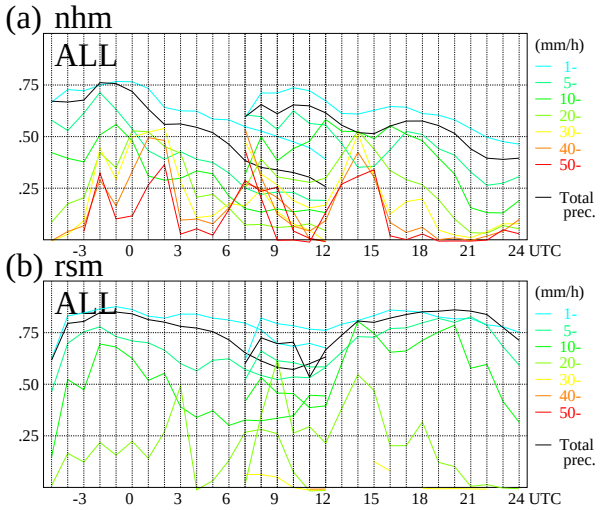

Fig.3 (a) Correlation coefficients for total precipitation amount and area between 5km-NHM (T=1-18 hours) and R-A. (b) Same as (a), but for RSM (T=7-24 hours).

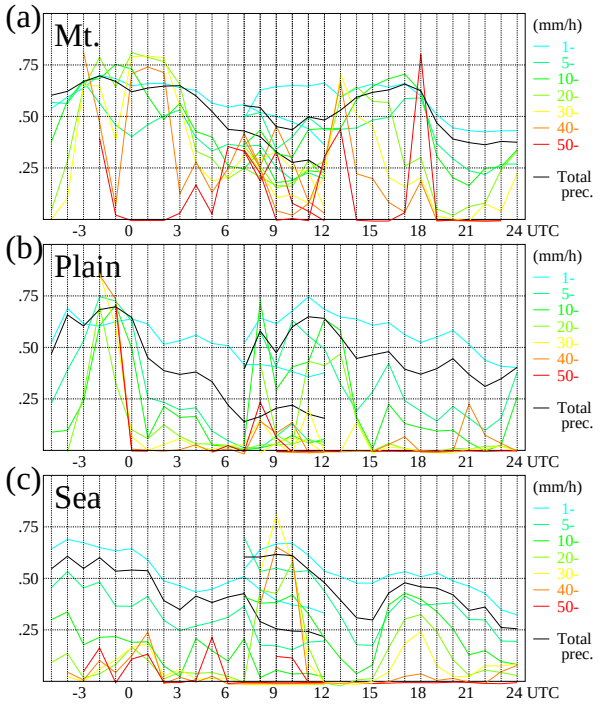

Fig.4 Same as Fig. 3a, but for (a) the mountainous, (b) plain, and (c) sea regions.

References

Kato, T., K. Kurihara, H. Seko, and K. Saito, 1998: Verification of the MRI-nonhydrostatic-model predicted rainfall during the 1996 Baiu Season. *J. Meteor. Soc. Japan*, **76**, 719-735.

Saito, K., T. Kato, H. Eito, and C. Muroi, 2001: Documentation of the Meteorological Research Institute / Numerical Prediction Division unified nonhydrostatic model. *Tech. Rep. Of the MRI*, **42**, 133pp.

Forecast of Sulfur Dioxide Flow from Miyake Volcano with a High Resolution Regional Transport Model

Hideaki Kawai
Numerical Prediction Division, Japan Meteorological Agency
(e-mail: h-kawai@met.kishou.go.jp)

1. Background

Mt. Oyama in Miyake Island (34.1N, 139.5E), which is located 180km south of Tokyo, erupted in July 2000. Even now a huge amount of sulfur dioxide which runs up to 10,000　20,000 t/day is discharged from the volcano every day. The emitted toxic gas occasionally spreads over Japan, depending on wind direction. The concentration of SO2 gas sometimes exceeds an environmental standard. The increase in concentration brings about nasty smell to us, damage to agricultural crops, increase in rejection rate of semiconductor production, and so on.

2. Model

For forecasting SO2 gas flow, we have newly developed a regional transport model which uses output from the Regional Spectral Model (RSM). RSM has a horizontal resolution of 20km and 40 vertical levels up to 10hPa.

The regional transport model adopts a Lagrangian approach, in which many tracer particles are released at the time and location of pollutant emission and displaced due to horizontal and vertical advection and diffusion. The model makes use of the 3-hourly model-level horizontal wind data of RSM, calculates the vertical wind on the hypothesis of hydrostatic equilibrium and advects each particle 3-dimensionally.

The vertical diffusion coefficient is decided following Mellor&Yamada's Level 2 Closure Model (Mellor and Yamada 1982) and each particle is displaced vertically on random walk process. In regard to horizontal diffusion, a random variation to the subgrid-scale turbulent velocity is given to each particle step by step following Langevin's equation (Gifford 1982).

3. Operation

Since June 2001, we have run the model up to 36 hours every day (00UTC initial) and JMA forecasters utilize products of the model for issuing two day forecast on SO2 gas from Miyake Volcano. The model assumes a constant SO2 emission from the initial time and uniform release from 0 to 1500m above the sea-level.

4. Examples of Forecast

The model forecasts generally show good agreements with the observed increase in SO2 concentration. Two examples are shown, in which SO2 gas reached far away.

Example 1: The model forecast starting from 00UTC 7 July 2001 predicted an inflow of SO2 gas into a channel between Shikoku Island and Kii Peninsula on 8 July 2001. High SO2 concentrations were observed at both sides of the channel on that day. The topography used in RSM and analysis of surface wind at 12UTC on 8 July 2001 is also shown (Fig. 1).

Example 2: The model forecast starting from 00UTC 15 August 2001 predicted a high concentration of SO2 gas on 16 August 2001 in Kyusyu Island, which is about 800km west from Miyake Volcano. High SO2 concentrations were observed in the central and eastern parts of Kyusyu Island on that day (Fig. 2).

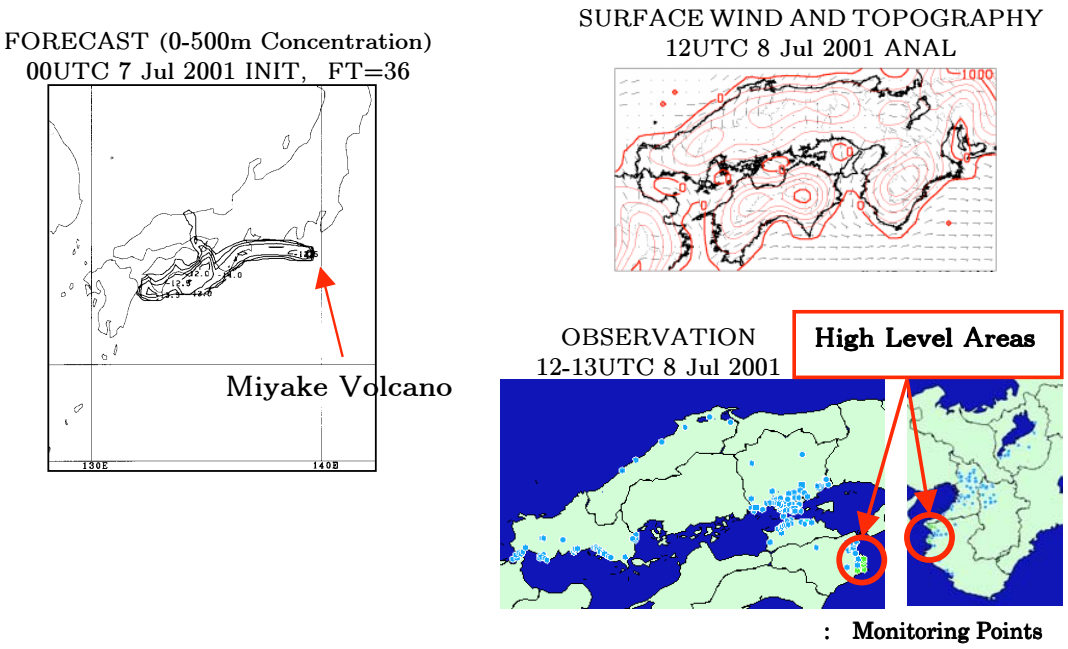

Fig. 1: An example of model forecast. The 36 hour forecast starting from 00 UTC 7 July 2001 is verified against the observation provided by the Ministry of the Environment of Japan. The upper right panel shows the surface wind analysis at the verification time and the model topography.

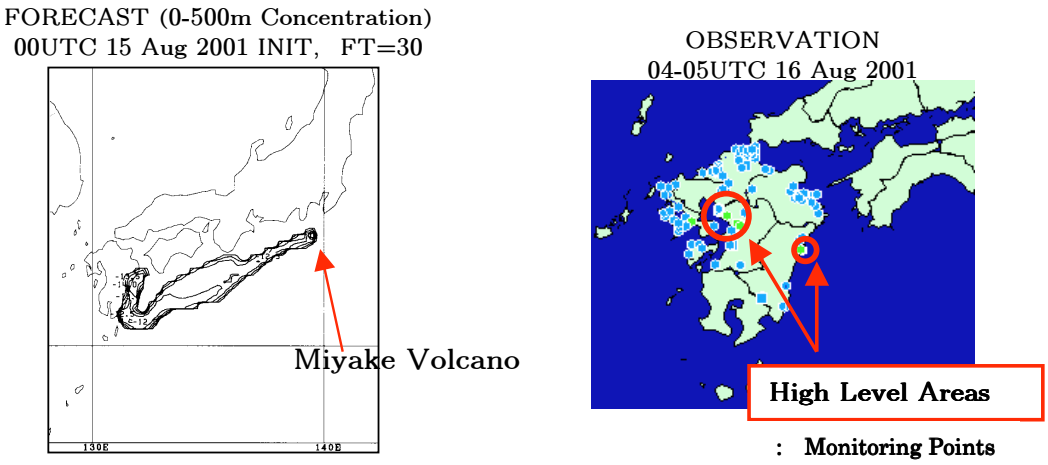

Fig. 2: Same as Fig. 1 except for the 30 hour forecast starting from 00 UTC 15 August 2001.

References

Gifford, F. A., 1982: Horizontal diffusion in the atmosphere: A Lagrangian-dynamical theory. *Atmos. Environ.,* **16**, 505-512.

Mellor, G. L. and T. Yamada, 1982: Development of a turbulence closure model for geophysical fluid problems, *Rev. Geophys. Space Phys.,* **20**, 851-875.

Numerical study of the 3-5 December 2001 intensive cyclone in Israel and eastern Mediterranean region

S.O. Krichak, M. Dayan, P. Alpert

Department of Geophysics and Planetary Sciences, Tel Aviv University
Ramat Aviv, Tel Aviv, 69978, Israel
shimon@cyclone.tau.ac.il

Unusually intensive rains characterized weather conditions over Israel during December 3-5, 2001. The rains were associated with a cold-core cyclone approaching the area from the west. The cyclone started its development over the Mediterranean Sea area several days prior to the period. Heavy rains were observed in Zichron Yaakov, of about 250 mm during the Dec.3 00:00 UTC – Dec. 5 00:00 UTC time period (192 mm per 6 hrs between Dec 04 06:00 LT and Dec 04 12:00 LT). At Maor station the precipitation amount was of about 70 mm per the 48 hours time period. The rainfall peak here was during 12:00-18:00 LT of December 4 with the rain intensity of about 20 mm per 6 hours. The weather developments were simulated with the MM5 mesoscale system adapted at Tel Aviv University NWP Unit for twice-daily real-time numerical weather prediction using two nested domains with 60 and 20 km resolution and 36 levels in vertical. The model runs are initiated by the NCEP and UKMO objective analysis and forecast data. The daily model predictions are available on website http://earth.nasa.proj.ac.il/mm5/current/.

The model quite accurately predicted the precipitation in Israel although the model predicted values were somewhat lower than the observed maxima (Fig. 1). The simulated rain intensity was higher in the higher resolution model runs. Most of the model-produced rains (Fig. 2) were of non-convective form. Convective precipitation was found mainly along the coastline. According to the NCAR/NCEP Reanalysis Project data on the Best Lifted stability Index, an area with high negative values of the index already existed over the Eastern Mediterranean (EM) to 00:00 UTC on Dec. 3, i.e. prior to the cyclone rapid intensification. This indicated a high level of instability of the air mass in the lower troposphere. The zone shifted eastward together with the cyclone. The model simulation of the period demonstrated rapid intensification of the cyclone occurring after southward displacement of a mid-tropospheric low characterized by a narrow zone of relatively mild stratospheric PV intrusion on Dec. 5 00:00 (Fig. 3). The potential vorticity (PV) pattern on the 350 K (about 200 hPa) isentropic surface also demonstrates occurrence of intrusion of the cold air masses from the extratropical stratosphere into the upper troposphere over the Mediterranean region (Fig. 4). The process evidently played an important role in the cyclone

intensification over the EM. Analysis of the modeling results suggested important additional role, played by the local topography of the EM region, which resulted in the intensification of the low level flow in the narrow costal zone with the approach of the cyclone. The effect evidently caused a faster eastward propagation of the low-tropospheric system in advance of the more slowly moving upper-level trough.

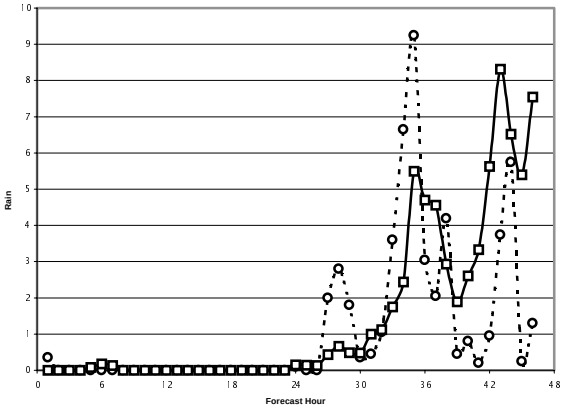

Fig. 1. Mean model produced (solid) and Observed (dashed) precipitation in northern Israel

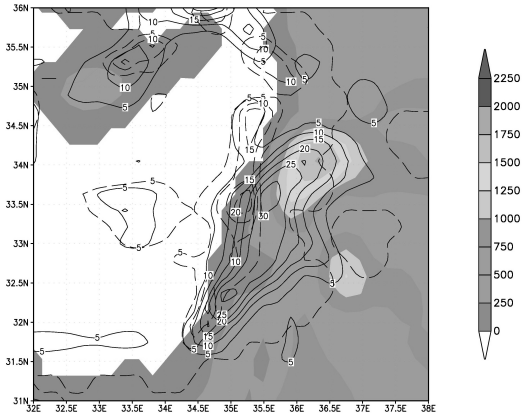

Fig. 2. Model terrain (shaded), convective (dashed) and non-convective (solid) precipitation at 00:00 UTC 05 Dec

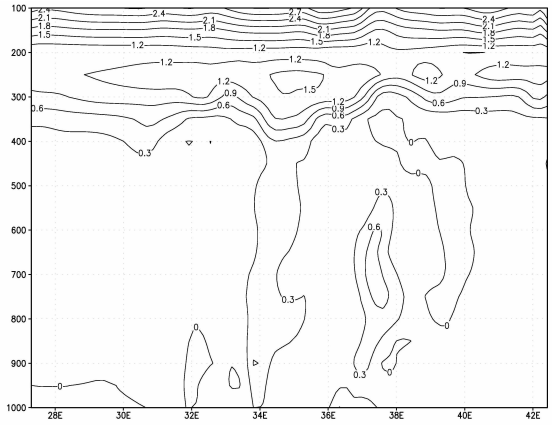

Fig. 3. PV cross-section along 35N at 00:00 UTC 5 Dec

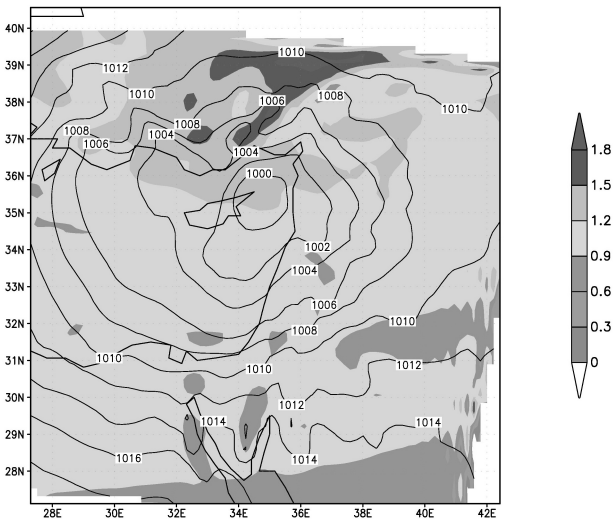

Fig. 4. IPV on 350K at 00:00 UTC 5 Dec 2001

THE NEW VERSION OF THE CANADIAN OPERATIONAL GEM REGIONAL MESOSCALE MODEL

Jocelyn Mailhot[1], Stéphane Bélair[1], André Tremblay[1], Louis Lefaivre[2], Bernard Bilodeau[1], Alain Patoine[2], Donald Talbot[2], and Anna Glazer[1]

[1] Meteorological Research Branch, [2] Canadian Meteorological Centre
Meteorological Service of Canada, Dorval, Québec, Canada
[1] e-mail: jocelyn.mailhot@ec.gc.ca

1. OVERVIEW OF NEW MESOSCALE SYSTEM

A regional version of the Global Environmental Multiscale (GEM) model has been operational for numerical weather prediction in Canada for some time. The last operational implementation of the regional version of the GEM model took place on 15 September 1998. It combined an increase in horizontal resolution (~ 24 km) with the Fritsch-Chappell convective scheme that resulted in significant improvements to the summertime QPF (Bélair et al., 2000). The operational model is run at the Canadian Meteorological Center (CMC) twice a day for 48 hours over North America and the adjacent oceans. The initial conditions at 0000 and 1200 UTC are provided by a regional data assimilation system (RDAS), with 12-h cycles using trial fields from 6-h regional integrations and a three-dimensional variational technique.

With the availability at the beginning of 2001 of two NEC SX-5 supercomputers, work began to prepare a new version of the mesoscale modeling system. The main changes to the mesoscale modeling system include an increase in both the horizontal and vertical resolution and major improvements to the physics package. The plans are to increase the number of vertical levels to 43 levels (instead of 28) and the horizontal resolution to 15 km in the uniform domain over North America. The modified physics package includes a new surface modeling system, an improved formulation of the cloudy boundary layer, changes to the convection and explicit schemes, together with revisions to the cloud radiative optical properties. Several changes to the current RDAS are also underway (see Chouinard et al., this volume).

2. THE NEW PHYSICS PACKAGE

The improved version of the physics package that has been developed for the mesoscale forecasting system is also being tested for a new mesocale global version of GEM.

2.1 *Surface processes*

The new surface modeling system aims at an improved treatment of surface processes, using a mosaic-type approach for vegetated land with possible snow pack, for ice-free and ice-covered oceans and lakes, and for glaciers.

A modified version of the ISBA (Interactions Soil Biosphere Atmosphere) scheme is used over land with special attention to the physics of snow to improve its wintertime performance (for details, see Bélair et al., this volume). The new system uses a high-resolution dataset to generate the needed geophysical fields (vegetation types, soil properties,…). A sequential assimilation method based on model error feedback of low-level air temperature and humidity has been developed to generate the soil variables (soil temperature and soil moisture at two levels).

Over sea ice, the surface temperature is obtained from a multi-level thermodynamic sea ice model based on a modified version of the model of Semtner (1976). Its main features comprise a snow cover on top of the ice, heat conduction through snow and ice, thermal inertia of the snow and ice layers, and a parameterization of albedo, conductivity and heat capacity (following Ebert and Curry, 1993 and Flato and Brown, 1996). The effects of leads in ice are also considered.

The sea ice model has been tested in stand-alone mode using datasets representing the climatology of the Arctic and from the SHEBA field campaign to simulate the annual and diurnal cycles over sea ice. In both cases, fairly good agreement with observations was obtained using a 3-layer version of the thermodynamic sea ice model (the uppermost of which may be snow).

2.2 *The cloudy boundary layer*

An improved formulation of the cloudy boundary layer, using a unified moist turbulence approach following the strategy of Bechtold and Siebesma (1998), has been developed. This formulation is appropriate for a low-order turbulence model such as our TKE scheme and allows a general description of stratiform clouds and shallow non-precipitating cumulus convection regimes using a single parameter Q_1 representing the normalized saturation deficit. Statistical relations appropriate to the various boundary-layer cloud regimes were obtained by Bechtold and Siebesma (1998) based on observations and large-eddy simulations, that permit to define the subgrid-scale cloud fraction and cloud water content in terms of Q_1 only. Preliminary tests with this

formulation on a case of Arctic boundary-layer clouds over a polynya observed during FIRE.ACE indicated much improved performance of the model.

2.3 *Condensation schemes*

An optimized version of the Kain and Fritsch (1990; KF) deep convective scheme is now being evaluated as a replacement to the Fritsch-Chappell (FC) scheme. The main improvement over the FC scheme comes from the one-dimensional entraining/detraining plume model for the updrafts and downdrafts, and from more detailed microphysics (including glaciation effects).

An explicit cloud scheme with mixed-phase (MXP) microphysics (Tremblay and Glazer, 2000) is being tested to replace the current Sundqvist scheme. The MXP cloud scheme was developed to incorporate more detailed microphysics into mesoscale models. The MXP scheme uses only one prognostic variable, the total cloud water content, making it simple enough to be used in an operational environment, yet it discriminates between the solid, warm, and supercooled liquid phases.

The explicit microphysical processes include condensation or evaporation of cloud droplets, evaporation of rain, ice nucleation, deposition or sublimation of ice particles, sedimentation, and ice melting. Sedimentation includes thresholds with values of the liquid water and ice content of 0.1 g m^{-3} and 0.01 g m^{-3}, respectively, to model the onset of precipitation. Homogeneous nucleation freezing of supercooled cloud droplets and raindrops at temperatures below - 35° C is also considered. For mixed-phase clouds in which both warm and cold microphysical processes are active, the partition between liquid and ice is based on a diagnostic equilibrium relation for the ice fraction within saturated updraft in the cloud. This equilibrium solution expresses the steady-state balance between riming, vapor deposition, production of vapor excess by adiabatic cooling, and mixed-phase sedimentation. The adiabatic cooling process depends on the vertical velocity representing an explicit forcing of microphysical processes by the model dynamics.

2.4 *Cloud optical properties*

Revisions to the cloud optical properties have been made in order to improve cloud-radiation interactions. The revised broadband solar and infrared parameters (extinction coefficient, single-scattering albedo, asymmetry factor) are based on the models of Hu and Stamnes (1993) for cloud water and Fu and Liou (1993) for ice crystals. The effective radius of hydrometeors, a crucial parameter for the cloud optical properties, now varies between 2.5-60 μm for cloud droplets, and 20-150 μm for ice particles depending on the mass and temperature. The lower values of effective radius used in the current scheme generally resulted in too much solar attenuation by clouds.

3. CURRENT STATUS

Due to the large number of modifications proposed for the new mesoscale forecast system, it was decided to proceed in two steps for its parallel testing and operational implementation at CMC. First, only the new surface modeling system together with its sequential assimilation of surface variables, without any changes to the model resolution, was put in parallel runs at CMC during the summer 2001 and was implemented in September 2001.

Verifications showed that the new surface modeling system greatly contributes to improve the representation of temperature and humidity fields, mostly at lower levels, and to improve the diurnal cycle of surface air temperature and the objective precipitation scores (cf., Bélair et al., this volume).

The rest of the changes (increased horizontal and vertical resolutions, new condensation package, and revisions to cloud optical properties) will be put subsequently in parallel runs. Preliminary tests of the impact of those changes have recently begun. Current plans are for operational implementation early in 2002.

4. REFERENCES

Bechtold, P., and P. Siebesma, 1998: Organization and representation of boundary layer clouds. *J. Atmos. Sci.*, **55**, 888-895.

Bélair, S., A. Méthot, J. Mailhot, B. Bilodeau, A. Patoine, G. Pellerin, and J. Côté, 2000: Operational implementation of the Fritsch-Chappell convective scheme in the 24-km Canadian regional model. *Wea. Forecasting*, **15**, 257-274.

Kain, J.S., and J.M. Fritsch, 1990: A one-dimensional entraining/detraining plume model and its application in convective parameterization. *J. Atmos. Sci.*, **47**, 2784-2802.

Tremblay A. and A. Glazer, 2000: An improved modeling scheme for freezing precipitation forecasts, *Mon. Wea. Rev.*, *128*, 1289-1308.

Limited Area Predictability: Can "Upscaling" also Take Place?

Fedor Mesinger*, Keith Brill^, Hui-ya Chuang+, Geoff DiMego#, and Eric Rogers#

* NCEP/EMC and UCAR; ^ NCEP/CPC; + NCEP/EMC and SAIC; # NCEP/EMC, Camp Springs, Maryland

Introduction. A standard situation in all major forecasting centers is the existence of a global and of at least one regional, or "limited-area" forecasting system, with the latter using the lateral boundary data forecast by the former. Yet, the strategies as to what is apparently expected of the limited-area models (LAMs) can be radically different. For example, at the U.K. Met Office (Fig. 1, Staniforth 2001) and at various ALADIN partners (Fig. 1, Members of the ALADIN international team 1997) LAM domains of the order of 2000 x 2000 km and even smaller are used. In contrast, the operational Eta at NCEP is run on a domain greater than 11500 x 8500 km. Is this done to have "the contamination at the lateral boundaries" (Laprise et al. 2000) as far away from the region of interest as possible, or does the Eta strategy imply an attempt to achieve not only downscaling, but an improvement in the large scales as well?

An additional factor in the Eta operational setup is that its lateral boundary condition is obtained from the previous run of the global (Avn) model, which is at the "on" times (00 and 12z) estimated to represent about an 8 h loss in accuracy. It takes a day or two at the most for some of the forecast jet-stream entering the western Eta boundary to reach the region of most interest, the contiguous United States. Shouldn't then at later forecast times the skill of the Eta fall behind that of the Avn of the same initial time? Recent extensions of the Eta forecasts at NCEP to 60 h and then, in April 2001, to 84 h, have much improved the possibilities for looking into these issues. We here present and summarize the results of three efforts in that direction: examination of precipitation threat scores, of the rms fits to raobs, and of the accuracy in placing the centers of major storms at later forecast times.

Precipitation scores. It was pointed out earlier that out to 48 h, and then out to 60 h (Fig. 5, Mesinger 2001) no signs of the deterioration of the Eta precipitation threat scores compared to those of the Avn were evident. At the time of this writing nine full months are available of the Eta scores out to 84 h. In Fig. 1 these nine months, May 2001-January 2002, of the Eta and the Avn threat scores are shown, for the sample of 00-24, 12-36, and 24-48 h, left panel, and that of the 36-60, 48-72, and 60-84 h forecasts, all verifying at 12z, right panel. There are more than 700 verifications in each of the panels. The advantage of the Eta over the Avn in the forecast periods going beyond the two days is seen to have remained overall just about the same as it was in the up to two day periods.

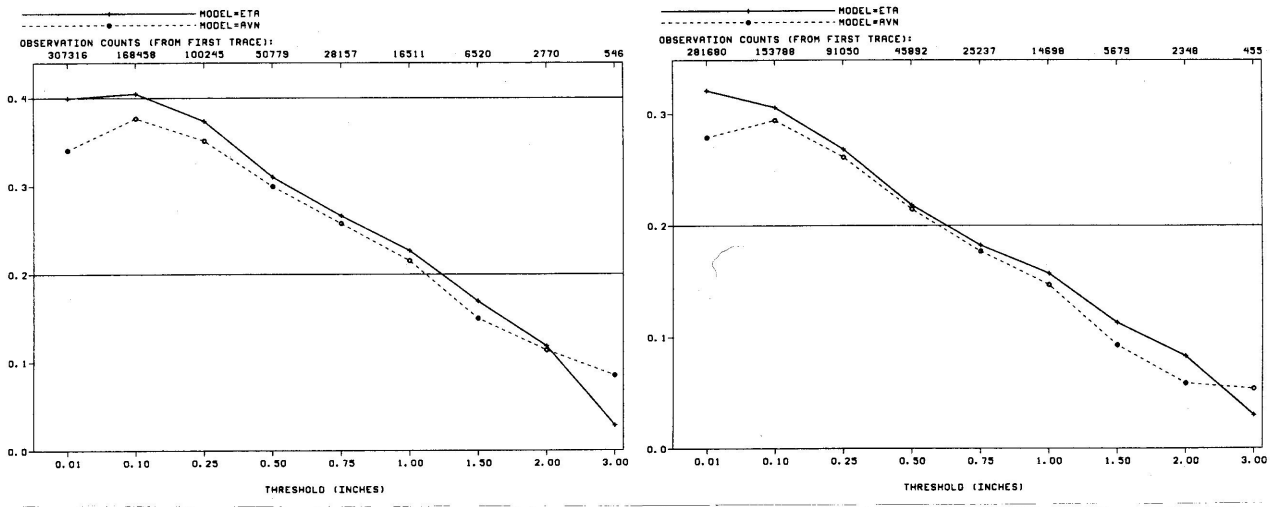

Fig. 1. Equitable precipitation threat scores of the Eta (solid) and the Avn (dashed lines), 00-24, 12-36, and 24-48 h forecasts, left panel, and 36-60, 48-72, and 60-84 h forecasts, right panel, May 2001-January 2002.

* *Corresponding author address*: Fedor Mesinger, NCEP Environmental Modeling Center, 5200 Auth Road, Room 207, Camp Springs, MD 20746-4304; e-mail: fedor.mesinger@noaa.gov

RMS fits to raobs. EMC Forecast Verification System offers numerous possibilities for compilation of various statistics of NCEP model forecasts' fits to data. RMS fits to raobs for the last 30 days for four forecast variables, including 250 mb winds, 500 mb heights, and 850 mb temperatures, are posted at http://sgi62.wwb.noaa.gov:8080/VSDB/. In compiling those, each model results are interpolated to an output grid; the Avn is interpolated to an 80-km grid ("211") while the Eta is interpolated to a 40-km grid ("212"). This presumably favors the Avn, but should not affect much the "error growth" rate.

Plots of the rms fits to raobs of the three variables mentioned, for spring 2001 out to 60 h, and for the summer 2001 out to 84 h, have been shown in Mesinger et al. (2002). No general tendency of the Eta "errors" to increase at later forecast times faster than those of the Avn was seen. In Fig. 2 we show rms plots for 250 mb winds, left panel, and 500 mb heights, right panel, for 00 and 12z verifications during December 2001-January 2002, the two full months of winter 2001-2002 available at the time of this writing. Even though in winter the inflow of the lateral boundary information is the fastest, the Eta "error growth" after 60 h happens to be in fact on both plots somewhat slower than that of the Avn's.

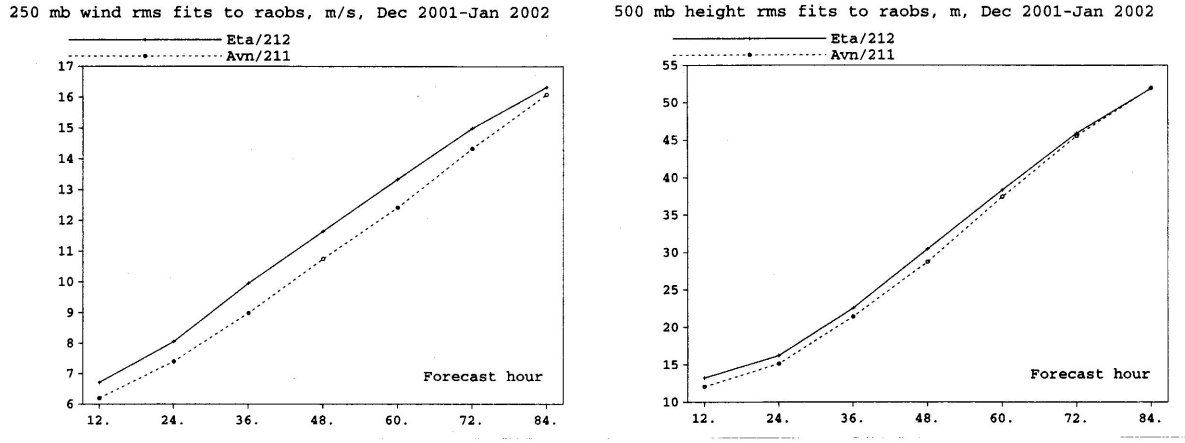

Fig 2. RMS fits to raobs, 250 mb winds (m/s, left) and 500 mb heights (m, right panel), for the Eta (solid) and the Avn (dashed lines) models, as a function of forecast hour, December 2001-January 2002.

Placing the centers of major storms. In (Mesinger et al. 2002) rules were set up for identification of major surface lows, and the accuracy of the Eta and the Avn in forecasting the positions of these centers at 60 h forecast time during December 2000-February 2001 was inspected. It was found that the Eta was considerably more accurate, winning about 2/3 of the 31 cases identified, and having a 100 km smaller median error. But when one case was rerun by the Eta switched to use the sigma coordinate (Fig. 2, Mesinger et al. 2002) the position error, at 48 h, increased from 215 to 315 km.

Concluding comments. Results shown and summarized indicate that the Eta is able to compensate for the inflow of the less accurate "old" Avn boundary condition, so that out to 3.5 day forecast time it remains competitive with the Avn of the same initial time. One experiment referred to suggests that the eta coordinate is a significant contributor to this ability.

The large-scale character of the various statistics presented and cited indicates that the Eta is indeed generally improving on the largest scales it can accommodate in its relatively large domain, of about 1/5 of the globe, over the Avn information it is receiving at its lateral boundaries.

References

Laprise, R., M. R. Varma, B. Denis, D. Caya, and I. Zawadzki, 2000, *Mon. Wea. Rev.*, **128**, 4149-4154.

Members of the ALADIN international team, 1997, *WMO Bull.*, **46**, 317-324.

Mesinger, F., 2001, *50th Anniversary of Numerical Weather Prediction Commemorative Symposium*, A. Spekat, Ed., European Meteor. Soc. (Carl-Heinrich-Becker-Weg 6-10, 12165 Berlin, Germany), 91-118.

Mesinger, F., K. Brill, H.-Y. Chuang, G. DiMego, and E. Rogers, 2002, *Symp. on Observations, Data Assimilation, and Probabilistic Prediction*, Orlando, FL, Amer. Meteor. Soc., J36-J41.

Staniforth, A., 2001, *50th Anniversary of Numerical Weather Prediction Commemorative Symposium*, A. Spekat, Ed., European Meteor. Soc. (Carl-Heinrich-Becker-Weg 6-10, 12165 Berlin, Germany), 185-200.

LEPS, the Limited–area–model Ensemble Prediction System at ARPA-SMR

Chiara Marsigli, Andrea Montani, Fabrizio Nerozzi,
Tiziana Paccagnella and Stefano Tibaldi

ARPA-SMR, Bologna, Italy

The Ensemble approach allows to associate a probability of occurrence to meteorological events, providing further scope to quantitative precipitation forecasting. Current operational implementations of the ensemble prediction technique are currently based upon global circulation models essentially covering the global scale. In the limited–area model (LAM) environment, it appears to be difficult to produce perturbations of the initial conditions which can efficiently grow for time ranges longer than 12–24 hours, depending on the size of the integration domain, possibly due to the driving/damping effects of the lateral boundary conditions. One natural approach to regionalize and adapt the global–scale ECMWF Ensemble Prediction System (EPS) on the local scale should be to nest limited–area models in each EPS member. The obvious drawback of this procedure is connected to the large amount of computer resources required and to the intense data–flow necessary if the LAM integrations are not performed in the same centre where the EPS is produced.

At the Regional Meteorological Service of Emilia–Romagna (ARPA-SMR, in Bologna, Italy) the dynamical adaptation of the EPS on the local scale through LAM nesting, is founded on an ensemble reduction technique where only few members of the entire global ensemble are selected to drive LAM integrations (Molteni et al., 2001; Marsigli et al., 2001). The reduction procedure is carried on by performing, on a restricted area (53–35N; 5W–25E), an independent cluster analysis of the 51 EPS members by a complete linkage method, where clustering is based on dynamic and thermodynamic fields in the lower–to–middle troposphere. The number of clusters is fixed to 5. A Representative Member (RM) for each of the 5 clusters is then defined by selecting the cluster member with the minimum distance from the other members of the same cluster and the maximum distance from all the remaining EPS members. These 5 RMs provide initial and boundary conditions for 5 LAM integrations up to three-to-five days ahead. The 5 individual LAM integrations are then used to compute a–priory probability of occurrence of meteorological events of interest, e.g. the exceeding of a given accumulated precipitation threshold, by combining them with weights proportional to the population of the cluster they represent.

Another practically important feature of the ARPA-SMR methodology is the use of the concept of "super-ensemble". Rather than using only one ECMWF EPS set, more (up to three) consecutive daily EPS sets, progressively lagged in time, are used, providing initial sets of up to 153 individual members. From preliminary evaluations, the use of the super-ensemble technique increases the reliability of the computed a-priory probability of occurrence of the predicted event (surpassing of a precipitation threshold). The LAM employed so far is LAMBO (Limited Area Model BOlogna), the hydrostatic limited-area

model in operational use at ARPA-SMR. LAMBO is based on the NCEP ETA model and has an operational horizontal resolution of 10 or 20 km with 32 vertical levels.

The LEPS technique is under evaluation on a set of individual case studies of severe precipitation events in Europe. In the following figure, an example of the results of the LEPS application is shown in the case of the Soverato flood event (September 2000), which occurred in the Calabria region (the "tip" of the "Italian boot"). Precipitation exceeding 340 mm/day was observed in the land areas of the Calabria region, this causing landslides, great disruption and losses of life. Fig.1 shows the rainfall probability maps (exceeding the 20 and 100 mm/day thresholds) generated by the super–ensemble methodology 60 hours before the event. Both localisation and intensity of the flood are properly captured, despite the fact that these maps are obtained by combining only 5 (weighted) LAMBO integrations (Montani et al., 2002).

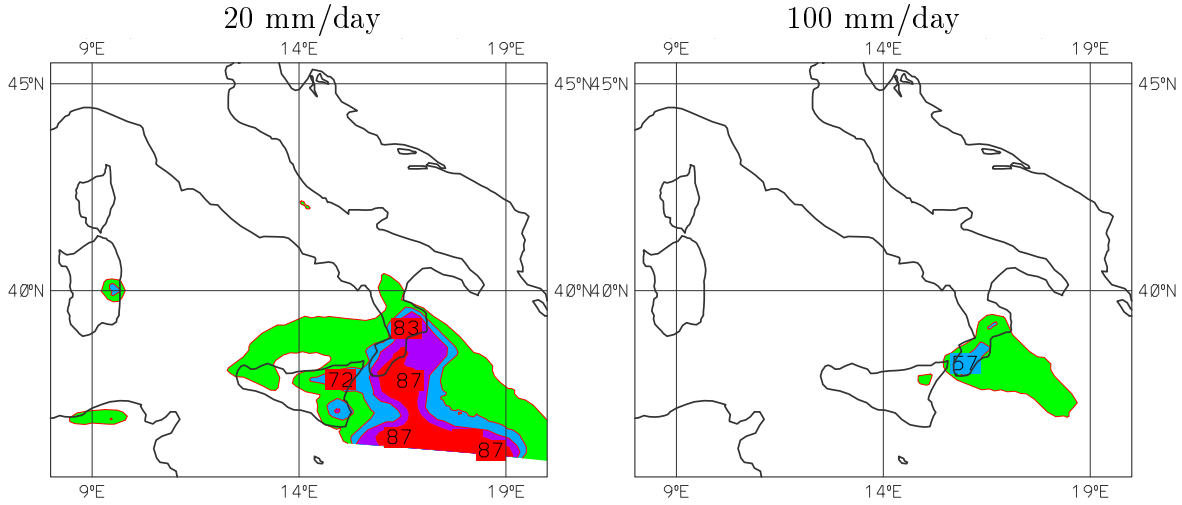

Figure 1: Probability maps (valid at 00UTC 10 September 2000; 60 hour forecast) for 24h accumulated rainfall exceeding 20 and 100 mm (left and right panel, respectively) as predicted by the super–ensemble. Contours every 20%.

Currently, the LEPS technique is still being tested and developed. The first major change will involve the type of LAM employed, since the non–hydrostatic Lokal Modell replaces LAMBO. The name of the project will also reflect this change, from LEPS to COSMO–LEPS, to officially frame this project in the COSMO (COnsortium for Small–scale MOdelling) project. During 2002, COSMO–LEPS will be tested on a quasi–operational basis, to allow a comprehensive verification effort, based on subjective and objective criteria.

References

Marsigli, C., Montani, A., Nerozzi, F., Paccagnella, T., Tibaldi, S., Molteni, F., Buizza, R., 2001. A strategy for High–Resolution Ensemble Prediction. Part II: Limited-area experiments in four Alpine flood events. *Quart. J. Roy. Meteor. Soc.*, **127**, 2095–2115.

Molteni, F., Buizza, R., Marsigli, C., Montani, A., Nerozzi, F., Paccagnella, T., 2001. A strategy for High–Resolution Ensemble Prediction. Part I: Definition of Representative Members and Global Model Experiments. *Quart. J. Roy. Meteor. Soc.*, **127**, 2069–2094.

Montani, A., Marsigli, C., Nerozzi, F., Paccagnella, T., Buizza, R., 2002. Performance of the ARPA–SMR limited–area ensemble prediction system: two flood cases. *Nonlin. Proc. Geophys.*, in press.

Improved atmospheric boundary layer model for operational short-range forecasting

Shnaydman V.A.
Department of Environmental Sciences,Rutgers University-Cook college 14College Farm Road New Brunswick, NJ, 08901 USA
e-mail:volf@envsci.rutgers.edu
Berkovich L. V., Tkacheva Yu.V.
Hydrometeorological Research Center of Russia,
e-mail: berkovich@rhmc.mecom.ru

The basic conception of the Hydrometeorological Research Center (HMRC) of Russia system for operational short-range forecasting is the reconstruction of both synoptic-scale and mesoscale weather patterns from the output product of a large-scale prediction scheme by atmospheric boundary layer (ABL) model and parameterization procedures (1,2). The results of the reconstruction of the ABL internal structure from objective analysis ad forecast data demonstrate the possibility of using the ABL model in operational prediction of meteorological fields and weather phenomena for a limited area encompassing Russia, Eastern Europe. Simultaneously these results showed the necessity of the improvement of the quantitative description of ABL turbulence structure. Let's remind that the mentioned above results were obtained by using the simplified turbulence closure scheme. It's supposed that the deficiencies are related on the simplification of the turbulence closure scheme. The two-equations closure scheme is used but the equations of turbulent kinetic energy and dissipation rate are written in time-dependant one-dimensional form. The missing terms seem to be represented the physical processes which have to be incorporated in the model realization.

The improvement of ABL model concerns the transport of the turbulent kinetic energy and dissipation rate, the production due to horizontal turbulent exchange. These effects are included in the closure scheme. The horizontal turbulent terms in the equations of the motion are described by the deformations of velocity. The capture of the missing terms in the equations of the turbulent kinetic energy and dissipation rate demands to rewrite the numerical algorithm. The finite-difference form of these equations in one-dimensional version is written in such way that the unknown functions of turbulent kinetic energy and dissipation rate have to be positive. Now it's done with taking into account the transport terms.

The comparison of the results obtained with unimproved and improved schemes shows that the improvements considered give essentially differences of turbulent characteristics and velocities of the organized motions. It means that the terms of the turbulent kinetic energy and dissipation rate transport are important for description the ABL turbulence structure.

The results of the improved model calculations show the better agreement with the measured data of meteorological fields. But these results are obtained only for small number of cases. The verification of the improved model is in progress.

Now we consider the ways to take into account the results of (3,4) for including the pressure correlation mechanism in the formation of the ABL turbulence structure. We use the parameterization scheme of the pressure-correlation which includes the turbulence-turbulence and mean fields-turbulence interactions. The two-equation turbulence closure scheme allows to calculate the both parts of the pressure-correlation term by using the Kolmogorov-Prandtl and Smagorinsky relationships and eddy-viscosity approximation. The use

of the algebraic expressions of Reynolds stresses obtained from simplified third moments equations is in the discussion. The dynamical interaction between underlying surface and atmospheric transfer with two characteristics of the relief (the heights and the slopes of the obstacles), with introduction of the effective roughness and urban effects will be also captured.

The ABL model improvements will be connected with further developments of the other modules of the Dynamical Weather Forecasting System operated in HMRC. The modeling algorithms will describe the humidity prediction through the implementation a land surface hydrology circle, the impact of atmospheric fronts upon the evolution of the meteorological variables in the boundary layer and free atmosphere.

REFERENCES

1.Berkovich L.V., Belousov S.L , Tkacheva Yu.V. Operational hydrodynamical forecasting of meteorological variables and weather patterns for locations in Russia and contiguous countries. – Russian Meteorology and Hydrology, 1998, No.4, 11-22.

2.Berkovich, L.V., Tarnopolskii, A.G., Shnaydman, V.A.: 1998, ‘Reconstruction of the Internal Structure of the Atmospheric Boundary Layer from Operational Meteorological Data,’ Russian Meteorology and Hydrology 7, 22-31.

3.Canuto,V.M.:1994,”Large Eddy Simulation of Turbulence: a subgrid model including shear, vorticity, rotation and buoyancy.” Ap.J.,428,729-752

4.Ying,R., Canuto,V.M.:1997, “Numerical Simulation of Flow over Two-dimensional hills Using a Second-order Turbulence Closure Model” Boundary Layer Meteorol.,84,447-474

A Z-Coordinate Version of the Non-Hydrostatic Model LM in Three Space Dimensions

J, Steppeler* and H. W. Bitzer**
*DWD, Offenbach , **AWGeophys , Traben Trarbach
E-mail: juergen.steppeler@dwd.de
Heinz-Werner.Bitzer@dwd.de

Meso γ scale models in terrain following coordinates generate strong erroneous forces near mountains, which lead to artificial circulations even with a horizontally stratified atmosphere. An obvious remedy of this problem is the use of a Z-coordinate, with the effect that the orography cuts into the lower model levels. With such an approach it is necessary to be careful in formulating the lower boundary condition. It is necessary to allow for a sufficiently smooth representation of the orography (see Kröner,1997). Step function representations of the lower boundary can have problems in representing the orography smoothly and therefore can produce problems in representing the flow around hills (Gallus and Klemp, 2000).

The approach presented here is based on the finite volume approach using shaved cells. These are obtained by cutting a regular rectangular grid with an orographic function which is represented as a continuous bilinear spline. A number of further approximations are applied in order to make the scheme practical for operational use.

Continuing our work on two dimensions, the scheme is implemented now in three space dimensions. A number of improvements were introduced as compared to the two dimensional version. Most important, the boundary values for the computation of the advection terms are computed by interpolating into the mountain using planes determined by three points which are outside the mountain.

A numerical experiment was performed using a circular mountain of height 400m and half width 10 km with 36 levels changing in thickness from 100m to 200m near the surface. The thickness of upper layers is 1200m. The horizontal grid length was 2 km. According to Gallus and Klemp (2000) the generation of a hydrostatic gravitational wave generated by a smooth bell shaped mountain is a crucial test for Z-coordinate models. Boundary treatments of the step mountain type often create solutions which are not very smooth and can even be entirely wrong.

Fig. 1a shows the u-velocity of the solution after 2.5 hrs, corresponding to a cross section through the centre of the mountain. It corresponds well to the terrain following solution of this problem, shown in fig. 1b.

Reference:

Gallus, W. and J. Klemp, 2000: Behaviour of flow over Steep Orography. *Mon. Wea. Rev.* **128**, 1153-1164.

Kröner,D., 1997: Numerical Schemes for Conservation Laws, Wiley, N. Y., pp507.

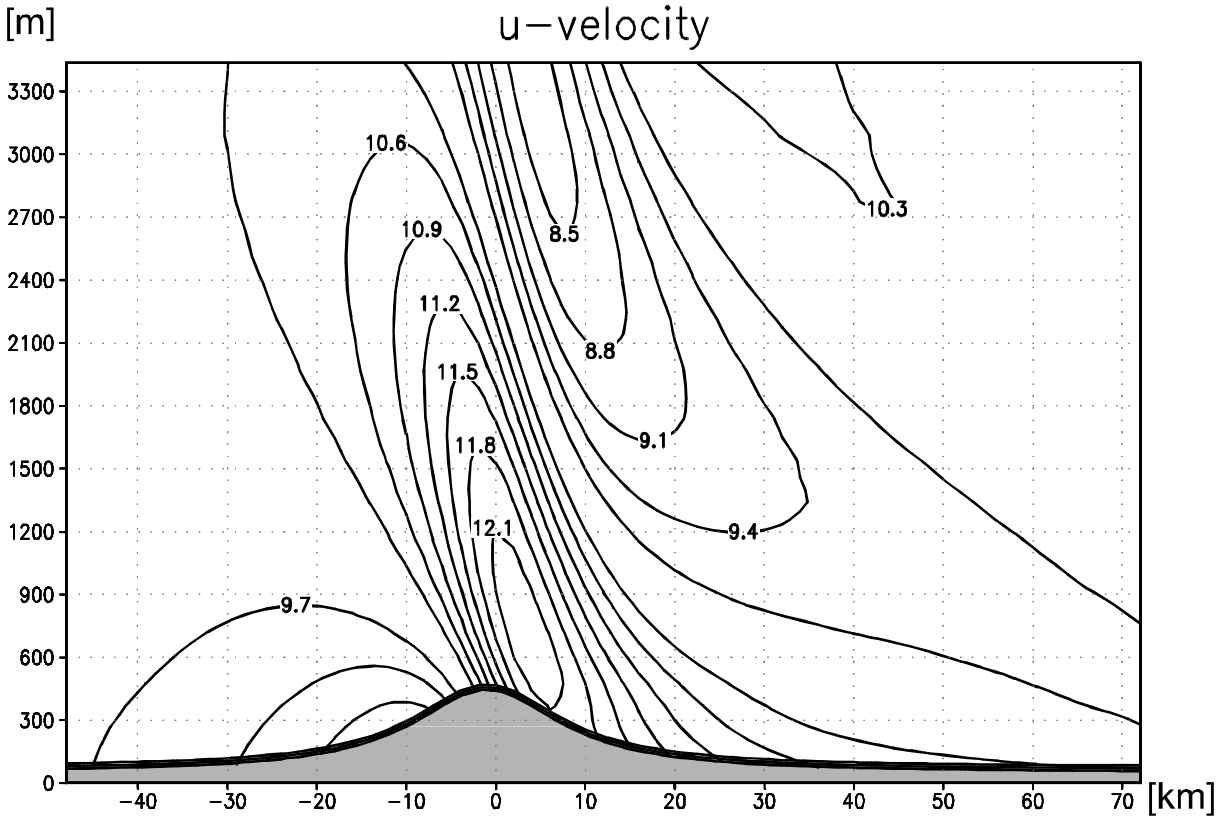

Fig. 1a: The u-velocity of the 2.5 hr forecast with the z-coordinate LM

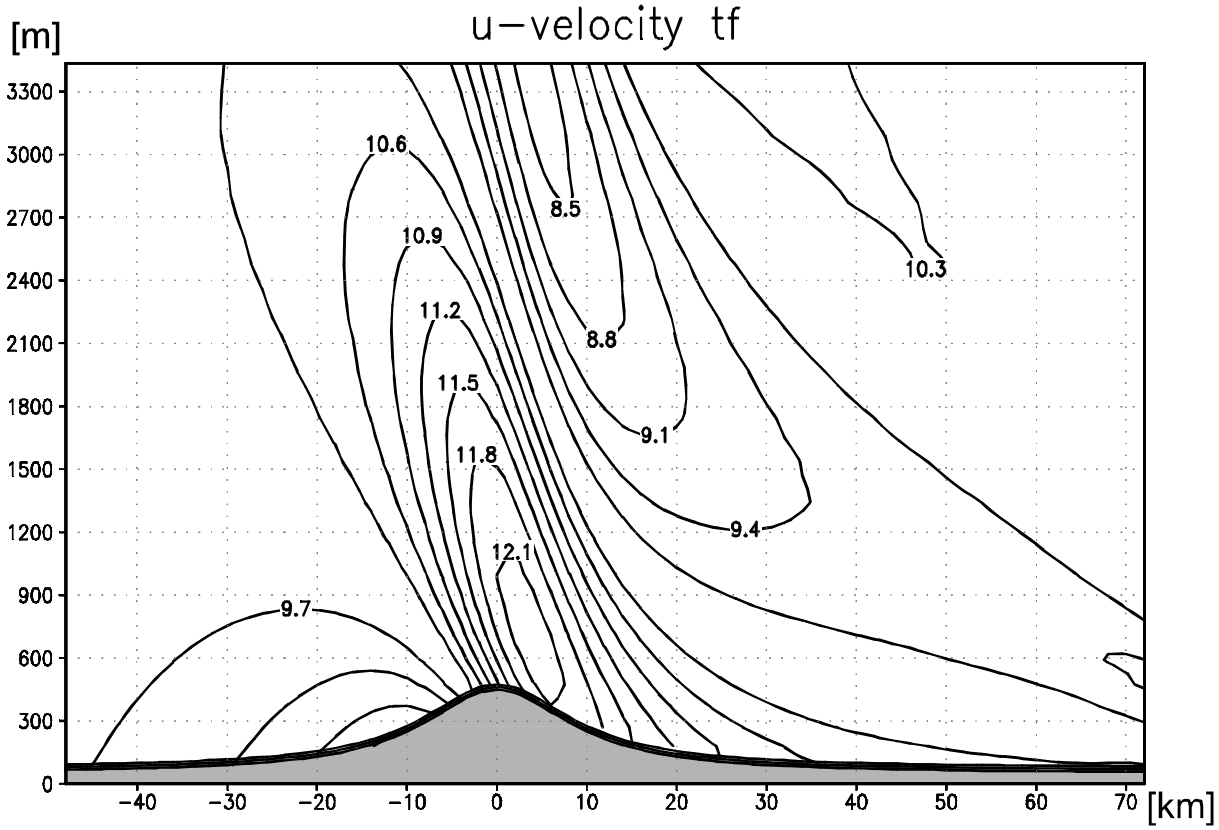

Fig. 1b: As fig 1a, for terrain following coordinate.

Pre-Operational trials of the new Met Office Mesoscale NWP Model

Clive Wilson *, Stephen Cusack, Byron Chalcraft, Martin Goeber, Jorge Bornemann,
Bruce Macpherson, Richard Renshaw, Adam Maycock, Nicola Robertson
Met Office, London Road, Bracknell, RG12 2SZ, U.K.

In spring 2002 the Met Office will update the formulation of the Unified Model which is used for mesoscale NWP. The formulation changes include both a new dynamical core for the model (Cullen *et al* (1997), (see also article by Davies et al in this issue)) and a some changes to the parametrizations package. The global model will also be changed to use the new dynamical core and updated parametrizations (see article by Milton et al in this issue) which will reunify the physics used in the operational global and mesoscale versions .

The new dynamics is a semi-implicit, semi-Lagrangian formulation and is non-hydrostatic . Height is the vertical coordinate and the horizontal and vertical grid staggering are different. In the vertical a Charney-Phillips grid staggering is used i.e. potential temperature and vertical velocity are now on the same half levels whereas everything else is held on the full levels. An Awakawa C grid staggering is utilised in the horizontal.

The changes to the physical parametrzations include: modifications to convection to a CAPE based closure and momentum transport; use of the gravity wave drag scheme with a flow blocking scheme. This is the first time that gravity wave drag has been included in the mesoscale model, and was found to have a small but beneficial impact on wind forecasts.

A series of trials have been carried out to compare the performance of the new model (NM) to that of the current operational mesoscale NWP model (OP). The current assimilation of satellite derived cloud and radar rainfall estimates though latent heat nudging are also included. A real time parallel trial has shown that, in general, the impact on forecasts has been small and neutral. The screen temperature and humidity have been significantly improved with a lessening of the cold and overmoist biases (Figure 1). The underforecasting of the 10m wind strength over the UK is also reduced .

During an anticyclonic period when there were several occasions of fog and low visibility the new model forecast visibility better. There was a tendency at the lowest threshold for increased bias but the false alarm rate was less affected than the hit rate so that the overall skil , as measured by the equitable threat score was substantially improved (Figure 2).

The implementation of the new dynamics with its non-hydrostatic capability will , in future, allow substantial improvements to both horizontal and vertical resolution to forecast weather and clouds better.

References

Cullen, M. J. P., T. Davies, M. H. Mawson, J. A. James, S. C. Coulter, and A. Malcolm, 1997: An overview of numerical methods for the next generation UK NWP and climate model. *Numerical Methods in Atmospheric and Ocean Modelling*, Lin, C. A., R. Laprise, and H. Ritchie, Eds., volume The Andre J. Robert Memorial Volume, 425–444.

 email: clive.wilson@metoffice.com

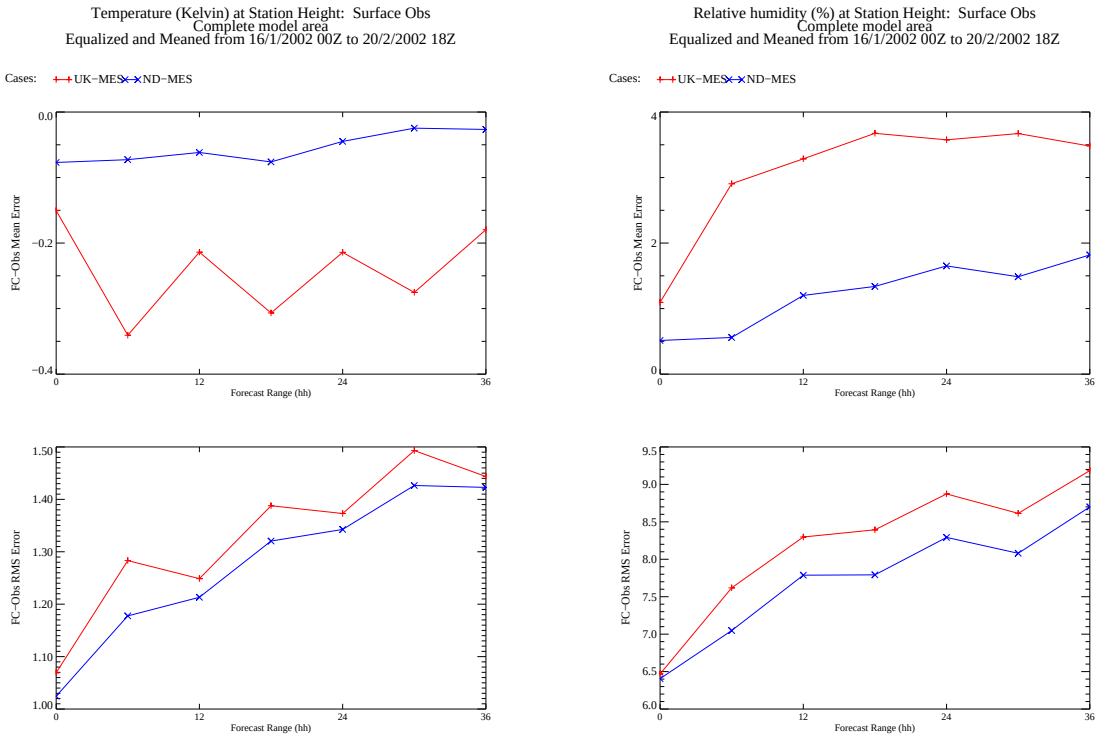

Figure 1: Screen temperature and humidity verification for NM (x) and OP(+); biases (top) and rms errors (bottom)

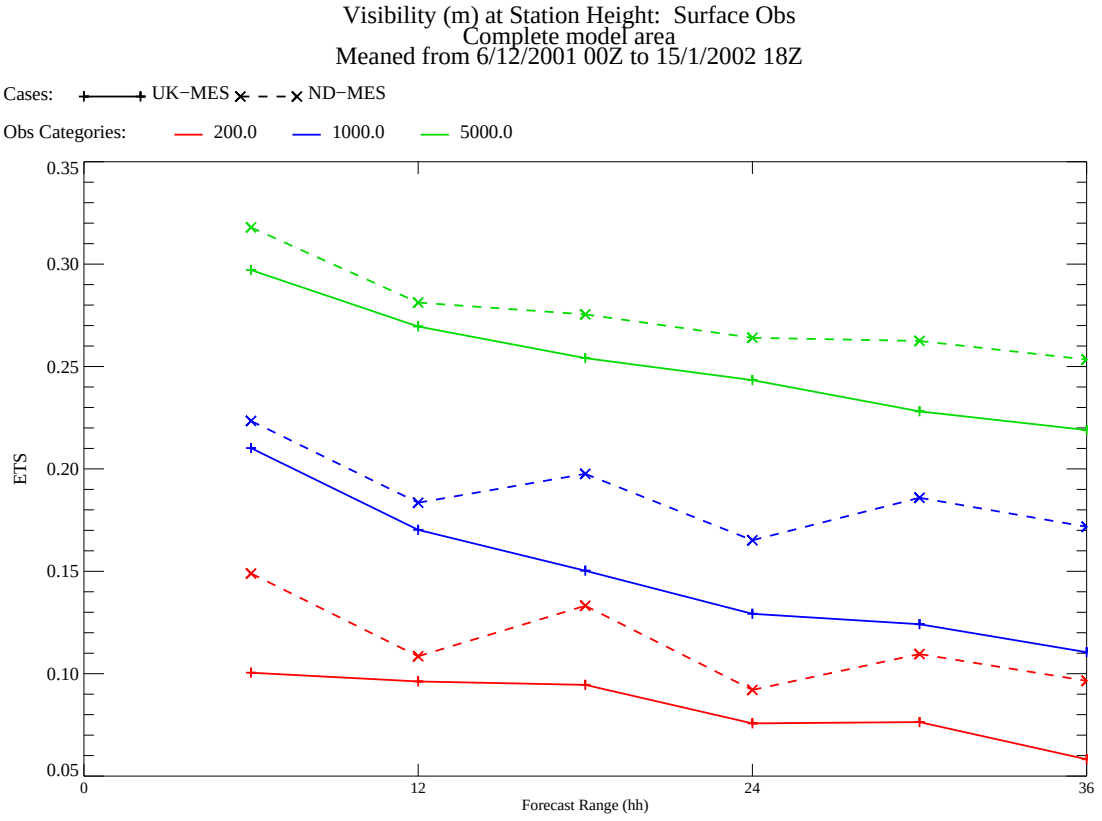

Figure 2: Equitable threat scores for visibility at 5km, 1km and 200m thresholds for NM (dashed) and OP (full)

A modified diffusion scheme for high-resolution simulations over mountainous terrain

Günther Zängl
Meteorological Institute, University of Munich, Germany
email: guenther@meteo.physik.uni-muenchen.de

1. Introduction

Most numerical models need explicit horizontal diffusion to ensure numerical stability. In mesoscale models based on a terrain-following coordinate system, the diffusion terms may introduce serious errors when they are calculated along the coordinate surfaces. The problem is most evident for atmospheric properties having a strong vertical gradient. Temperature diffusion along the coordinate surfaces, for example, tends to cool valleys and to heat mountains. Likewise, diffusion of the water vapor mixing ratio along the coordinate surfaces tends to dry valleys and to moisten the atmosphere above mountains. To prevent spurious temperature or moisture tendencies, diffusion should be computed truly horizontally. At sufficient distance from the ground, this can be accomplished with vertical interpolation between the coordinate surfaces. However, a special treatment is needed for the model levels close to the ground because a truly horizontal computation may be impossible without intersecting the ground. In the next section, an effective method to minimize diffusion-induced errors in the lower model levels is outlined. A more detailed description is given in Zängl (2002). The modified diffusion scheme has been implemented into the Penn State University/National Center for Atmospheric Research mesoscale model MM5. Test simulations presented in section 3 demonstrate that it greatly improves the model's capability of simulating complex flows in Alpine orography.

2. The modified diffusion scheme

In the modified diffusion scheme, diffusion is computed truly horizontally at all model levels where this is possible without intersecting the topography. For most variables, linear vertical interpolation between the coordinate surfaces appears to be sufficient. For the water vapor mixing ratio, however, exponential interpolation or a higher-order polynomial or spline interpolation should be used.

In the remaining model levels, diffusion is treated differently for momentum, temperature and the moisture variables. For momentum, a simple transition to diffusion along the coordinate surfaces (henceforth referred to as sigma-diffusion) is chosen. For the moisture variables (the mixing ratios of water vapor, cloud water etc.), a combination of one-sided truly horizontal diffusion and orography-adjusted sigma-diffusion is used. One-sided diffusion is discretized using the "half" of the centered difference scheme for the fourth derivative, i.e. $\left(\frac{\partial^4 u}{\partial x^4}\right)_i \approx \frac{3u_i - 4u_{i+1} + u_{i+2}}{\Delta x^4}$, Δx being the grid increment. Orography-adjusted sigma-diffusion follows the idea that sigma-diffusion may be applied along the axis of a valley without inducing spurious tendencies. However, in the direction across the valley axis, sigma-diffusion should be switched off. Details on this procedure are given in Zängl (2002). For temperature, orography-adjusted sigma-diffusion is used without one-sided truly horizontal diffusion because the latter damps slope wind circulations in an unphysical way. The sigma-diffusion for temperature is further improved by a correction involving the leading term appearing in the coordinate-transformed expression of the fourth-order diffusion operator.

3. A test simulation

Idealized numerical simulations of the valley wind system of the Alpine Inn Valley have been performed in order to test the modified diffusion scheme. The Inn valley has been chosen because a large amount of detailed measurements is available for this valley (e.g. Vergeiner and Dreiseitl 1987). Since these measurements show a lot of characteristic features recurring every fine weather day, the simulations could be based on a highly idealized setup, only orography being taken from data.

The test simulations have been computed on five interactively nested model domains, the finest horizontal resolution being 800 m. The innermost model domain covers the lower Inn valley together with its tributaries. In the vertical, 38 sigma levels are used, the lowermost one being located at about 18 m above ground. To keep the setup as simple as possible, the absence of any horizontal pressure and temperature gradients is assumed. This corresponds to vanishing large-scale winds. The simulation starts at a fictitious date of 15 October, 00 UTC (the date being relevant for radiation only) and is carried out for 30 hours. Temperature and moisture are specified according to what is typical for mid-October in the presence of continental air.

Three simulations based on the same initial conditions are considered. Two of them use existing model options. First, actual temperature (T) is used for computing the diffusion along the sigma levels. In the

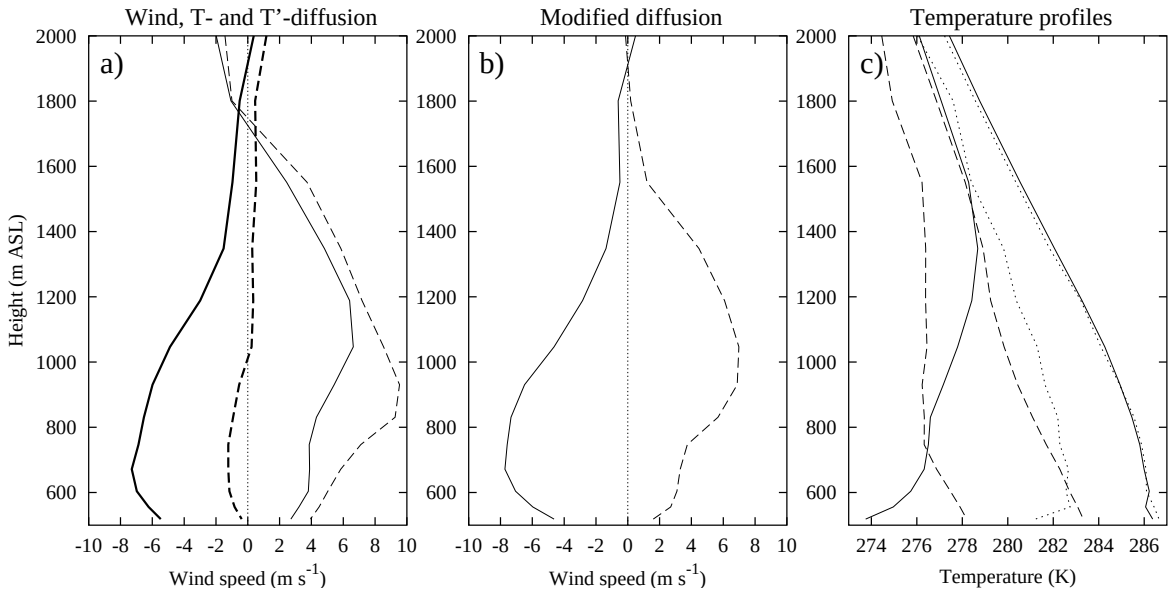

Figure 1: (a) Simulated wind profiles, $t = 16$h (solid lines) and $t = 30$h (dashed lines). Positive (negative) values denote downvalley (upvalley) wind. Simulations are performed with T-diffusion (thin lines) and T'-diffusion (bold lines). (b) Same as (a), but for simulation with the modified diffusion scheme. (c) Simulated temperature profiles for modified diffusion (solid lines), T-diffusion (dashed lines) and T'-diffusion (dotted lines). In each case, the colder (warmer) profile refers to $t = 30$h ($t = 16$h).

second simulation, the so-called perturbation temperature (T') is used for computing the diffusion. T' the difference between the actual temperature and a model reference temperature profile that usually has a vertical gradient around $-6\,\mathrm{K\,km^{-1}}$ in the lower troposphere. In the following, these two versions of sigma-diffusion will be referred to as T-diffusion and T'-diffusion, respectively. In the third simulation, the modified scheme described in section 2 is used.

Simulated vertical wind profiles at a location in the lower part of the Inn Valley are displayed in Figs. 1a and 1b for $t = 16$ h (solid lines) and $t = 30$ h (dashed lines). In each case, negative (positive) values denote upvalley (downvalley) wind. From the measurements, we expect upvalley wind in the afternoon and downvalley wind in the night. At the location considered here, the upvalley wind maximum is observed significantly closer to the ground than the downvalley wind maximum (see Zängl 2002 for more details).

It is obvious that the model fails to reproduce the observed valley wind circulation with the original sigma-diffusion scheme (Fig. 1a). With T-diffusion, downvalley wind is simulated throughout the day. It is only slightly weaker in the afternoon than during the night. On the other hand, permanent upvalley wind is obtained with T'-diffusion. It is rather weak at the end of the night and of realistic strength in the afternoon. With the modified diffusion scheme, however, the simulated valley wind circulation is rather close to reality (Fig. 1b). The wind maxima of both the upvalley wind and the downvalley wind are well within the observed range of values. Moreover, the observed day-night asymmetry of the height of the wind maximum is captured well by the simulation.

To explain the differences between sigma-diffusion and the modified diffusion scheme, vertical temperature profiles of the valley atmosphere are considered (Fig. 3). With the modified scheme (solid lines), a realistic diurnal temperature range is obtained. In particular, enhanced nocturnal cooling is evident up to a height of 1000 m above ground. Such a nocturnal temperature profile is rather typical for the Inn Valley (e.g. Vergeiner and Dreiseitl 1987). However, with sigma-diffusion, a realistic simulation of the diurnal temperature range is impossible. In both cases, the day-night difference of the surface temperature is several times too weak. Comparing the profiles for T-diffusion (dashed lines) and T'-diffusion (dotted lines), it becomes clear why the direction of the valley wind is opposite for these two options. With T-diffusion, the whole valley atmosphere is several degrees colder than with T'-diffusion.

References

Vergeiner, I., and E. Dreiseitl, 1987: Valley winds and slope winds – Observations and elementary thoughts. *Meteorol. Atmos. Phys.*, **36**, 264–286.

Zängl, G., 2002: An improved method for computing horizontal diffusion in a sigma-coordinate model and its application to simulations over mountainous topography. *Mon. Wea. Rev,* in press.